Integrated soil profile mapping reveals regional patterns of soil condition across Southern African agricultural lands

Trevan Flynn[a*], Andrei Rozanov[b], Samuel Mesele[c,d]

[a]Environmental Research Group, BrightGenesis Division, Add1Technologies, 11531 Slick Rock Dr., Richmond TX 77406 USA

[b]Department of Soil Science, Stellenbosch University, Private Bag X1, Matieland 7602, South Africa

[c]International Institute of Tropical Agriculture, Monrovia 1000, Liberia

[d]International Institute of Tropical Agriculture, Oyo Road, Ibadan 200001, Nigeria

*Corresponding email: t.flynn@add1technologies.com

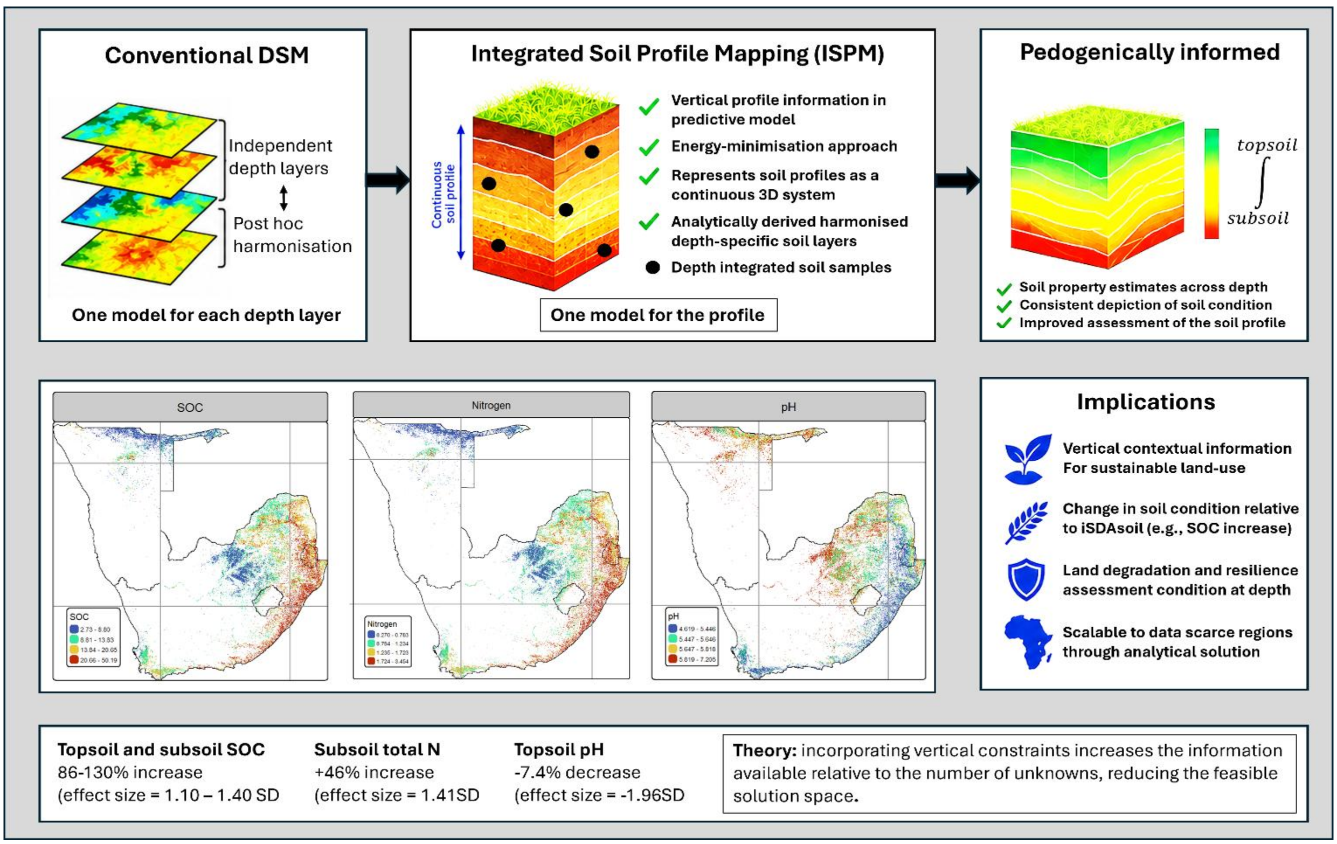

Abstract

Soil information at regional scales remains limited in Africa despite its importance for sustainable agricultural management, food security and land degradation assessment. Existing digital soil mapping approaches commonly model soil properties as independent depth layers and apply depth harmonisation after prediction, limiting their capacity to characterise changes in soil condition. Here, we present Integrated Soil Profile Mapping, a digital soil mapping framework that incorporates vertical profile information directly into prediction through an energy-minimisation approach. Integrated Soil Profile Mapping represents soil profiles as continuous three-dimensional systems and analytically derives harmonised depth-specific soil estimates. The framework was applied to seven soil properties including clay, pH, cation exchange capacity, soil organic carbon, total nitrogen, phosphorus and potassium using the Soils4Africa dataset across agricultural lands in Eswatini, Lesotho, Namibia and South Africa. Comparison with iSDAsoil revealed contrasting regional patterns in soil condition. Soil organic carbon increased by 86–130% (effect size = 1.10–1.40 SD), while subsoil total nitrogen increased by 46% (effect size = 1.41 SD). In contrast, topsoil pH declined by 7.4% (effect size = −1.96 SD), indicating substantial changes in soil biogeochemical condition. These patterns are consistent with differences in agricultural management and regional policy contexts, although attribution requires further investigation. The findings demonstrate the potential of vertically integrated soil mapping to characterise regional soil condition and provide a basis for monitoring environmental change, assessing soil resilience and supporting depth-driven sustainable land management across data-limited regions.

Keywords: Environmental Change; Food Security: Soil Information Systems; Soil Resilience

1. Introduction

Soil information at regional scales is fundamental to agricultural sustainability, food security and land management, yet Africa remains one of the most data-sparse regions globally for harmonised, quantitative soil information (Dewitte et al., 2013). The Soils4Africa project addresses this gap by providing a harmonised continental soil information system for agricultural lands, comprising approximately 20,000 observations distributed across Africa and designed to support repeated soil monitoring. Its spatially representative sampling framework builds on established approaches including the European Union Land Use Land Cover Area Frame Survey (LUCAS), the Land Degradation Surveillance Framework and the Africa Soil Information Service (Ballin et al., 2023; Leenaars et al., 2014). The hierarchical probability-based design enables statistical representation across heterogeneous environmental conditions and provides an important foundation for regional assessment of soil condition and its change (Kempen et al., 2021).

Despite its continental scale, the sampling design presents a key challenge for digital soil mapping. Soil observations are reported for only two broad depth intervals (0–20 and 20–50 cm), providing limited vertical resolution for reconstructing continuous soil profiles or deriving standardised depth intervals such as those used by GlobalSoilMap (Arrouays et al., 2014). This constrains the direct application of mass-preserving spline approaches, which generally require multiple observations at finer vertical resolution to characterise continuous depth distributions (Ponce-Hernandez et al., 1986). Consequently, conventional digital soil mapping (DSM) workflows face a structural limitation when harmonising sparse, broad-depth observations while preserving their vertical relationships.

Most DSM frameworks treat depth intervals as independent prediction targets, using spatial covariates derived from remote sensing, terrain and climate as primary predictors (McBratney et al., 2003). Vertical continuity is consequently often reconstructed after prediction through spline-based harmonization (Bishop et al., 1999; Malone et al., 2009; Ponce-Hernandez et al., 1986). While effective where observations provide sufficient vertical resolution, this separation of prediction and depth harmonisation can introduce additional uncertainty when profiles are sparse or coarsely discretised (Ma et al., 2021).

An alternative perspective is to treat soil predictions as a continuous vertical system rather than a collection of independent depth layers (Sharififar et al., 2026). Under this view, soil properties vary with depth according to pedogenic processes and can be represented through continuous depth functions (Kempen et al., 2011). Incorporating these profile-scale relationships directly within the modelling framework provides a means of maintaining vertical coherence between horizons while reducing reliance on post hoc harmonisation procedures.

The aim of this study was to develop an analytically solvable and vertically constrained DSM framework for mapping seven soil properties across agricultural lands in Eswatini, Lesotho, Namibia and South Africa. The framework prioritises vertical profile structure as an organising principle in soil prediction, complementing spatial covariates with profile-scale constraints to produce depth-consistent soil maps. Specifically, the objectives were to (i) develop a vertically coherent profile-mapping framework using Soils4Africa observations based on an energy-minimisation principle, (ii) evaluate its predictive performance and depth-harmonisation capability, and (iii) assess regional differences in soil condition between the resulting estimates and the iSDAsoil product. We hypothesised that the two soil information products would exhibit systematic differences in estimated soil condition due to differences in their underlying observations, modelling frameworks, sampling periods and the agricultural and environmental contexts represented by each dataset.

2. Materials and methods

2.1 Sites

Agricultural land occupies 292,478 km^2 across Eswatini, Lesotho, Namibia and South Africa, representing approximately 14% of the total land area (2,085,419 km^2) defined by the Soils4Africa land use delineation (**Fig. 1**a). The region spans a strong environmental gradient, including the tropical–subtropical conditions of the Caprivi Strip (Zambezi Province, Namibia), Mediterranean climates of the Western Cape (South Africa), semi-arid savannah systems in Eswatini and high-elevation temperate environments in Lesotho. Agricultural zones were highly fragmented and separated by major physiographic and ecological barriers, including the Namib and Kalahari deserts, the Succulent Karoo and Nama Karoo biomes, the Drakensberg and Cape Fold mountain ranges (Mucina and Rutherford, 2024), as well as extensive protected areas, mining regions and rapidly expanding urban centres. This strong heterogeneity in climate, lithology, topography and land use makes the region a robust testbed for evaluating soil mapping frameworks across multiple environmental regimes.

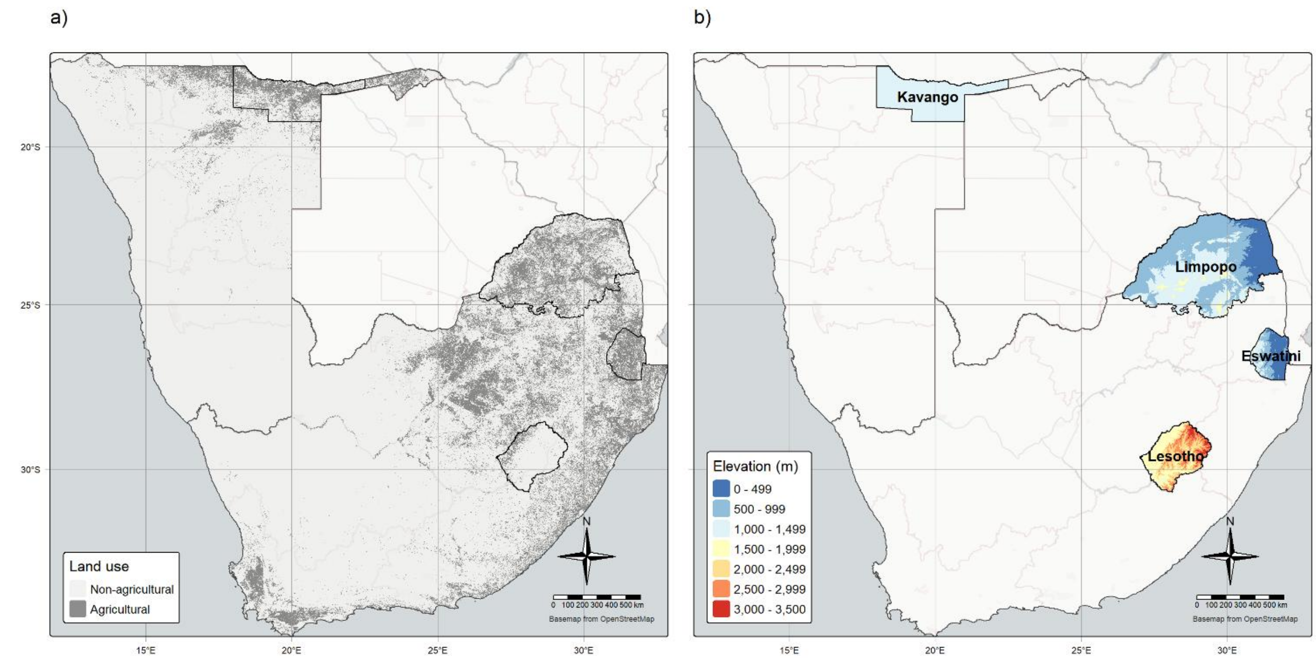

Fig. 1 *The agriculture area within Namibia, South Africa, Lesotho and Eswatini (a) and example regions due to the sparse agricultural land between the large land mass (b)*

The study modelled the whole area of agriculture land within the four nations, but example maps of four regions were given due to the diversity and spatial patchiness. Specific locations included Eswatini, Lesotho, Limpopo Province in South Africa and Kavango Province in Namibia (**Fig. 1**b). Specific soil property were selected within the example areas for the maps due to intrinsic relationships within the soil system.

2.2 Soil data

2.2.1 Soils4Africa

At the highest level, primary sampling units (PSUs) were defined by aggregating 100 m resolution agricultural land pixels into non-overlapping 2 × 2 km grid cells. Each PSU contained between 1 and 400 pixels classified as agricultural land. Within each PSU, agricultural pixels constituted the secondary sampling units (SSUs), which were further subdivided into 5 × 5 m tertiary sampling units (TSUs). A total of 5,000 PSUs were randomly selected, with allocation proportional to the extent of agricultural land in each country. Within each selected PSU, four SSUs were randomly chosen, and within each SSU, one TSU was selected, resulting in a total of 20,000 sampling locations. Backup locations were defined at each hierarchical level to ensure feasibility during field implementation (Kempen et al., 2021).

At each TSU, a composite soil sample was collected from four subsampling points arranged in a Y-shaped configuration, following the standardised field protocol described by Huising and Mesele (2022). This design ensured spatial representativeness at the local scale while maintaining consistency across the continental survey.

In the four countries of interest, during the year 2023, 1,614 samples (**Table. 1**) were obtained with a sampling density of 0.001 samples per km^2 throughout the agricultural land. Seven soil properties were selected for their influence on soil fertility and relationship to each other (**Table. 1**) including clay (g kg^{-1}), pH, cation exchange capacity (CEC; $cmol_c$ kg^{-1}), soil organic carbon (SOC; g kg^{-1}) total nitrogen (N; g kg^{-1}), phosphorus (P; g kg^{-1}) and potassium (K; g kg^{-1}).

Table. 1 *Summary statistics of Soils4Africa sampled data showing the mean, range, skewness and Kurtosis*

	Mean	Range	Skewness	Kurtosis
Clay (g kg^{-1})	316	10.0 – 690	-0.08	-1.12
pH	6.06	4.40 – 8.32	0.56	0.10
CEC ($cmol_c$ kg^{-1})	15.2	2.09 – 52.7	1.19	0.91
SOC (g kg^{-1})	13.9	1.30 – 54.6	1.36	1.79
N (g kg^{-1})	1.18	0.94 – 3.60	0.94	0.40

P (g kg^{-1})	15.3	2.49 – 104	2.74	11.7
K (g kg^{-1})	190	21.2 – 692	1.35	1.75

2.2.2 iSDAsoil

The Information Service for Data-Driven Agriculture (iSDAsoil) is a continental-scale African soil dataset developed to support data-driven agricultural applications through high-resolution digital soil mapping (Miller et al., 2021). The product was generated using ensemble machine-learning approaches trained on more than 70,000 soil observations compiled from government agencies, research institutions and non-governmental organizations across Africa. iSDAsoil was selected for comparison because it provides predictions for the same soil properties and equivalent depth intervals used within the Soils4Africa dataset, allowing direct comparison at a similar spatial support.

With the exception of effective cation exchange capacity (eCEC), all soil properties were either obtained directly or considered transferable between datasets. To estimate CEC comparably, exchangeable acidity predictions from Soils4Africa were added to the eCEC values from iSDAsoil rather than applying a pedotransfer function. This approach was chosen because most pedotransfer functions are calibrated for specific pedological conditions, whereas the study region spans multiple climatic gradients and soil-forming environments.

The iSDAsoil dataset was used as a baseline to determine if the soil condition has changed since the creation of iSDAsoil and the Soils4Africa measurements. Since the temporal distribution of soil samples in the iSDAsoil were obtained from different time periods, it was only used as a benchmark if the soil condition was changing and therefore, no temporal analysis was conducted.

2.3 Digital soil mapping theory

2.3.1 Integrated Soil Profile Mapping

Integrated Soil Profile Mapping (ISPM) is a DSM framework that explicitly incorporates vertical pedogenic structure into the predictive process. Unlike conventional DSM approaches that treat soil observations as independent depth intervals, ISPM represents the soil column as a continuous profile. The framework is governed by two primary principles. Firstly, a voxel integration fit for each prediction (pixel). This supplies continuous vertical constraints to the profile, allows for physically plausible depth predictions and allows for direct harmonisation. Second, a depth-support transformation, which redistributes the values from the profile scale to the horizon scale. Together, the voxel integral and depth-support transformation link the predictions to observable pedogenic behaviour.

During the predictions, the framework integrates vertical contextual information directly into the modelling domain by enforcing continuity of soil properties with depth, rather than relying solely on horizontal spatial covariates and post hoc depth harmonisation. In doing so, ISPM shifts the primary source of structural information from spatial dependency alone toward three-dimensional profile organisation. The energy-minimisation function governs how profile support is redistributed through depth under constrained assumptions. Essentially, it finds the path that needs the least energy to transition from one horizon value to the next (Flynn et al., 2026).

Within this formulation, soil horizons are derived from a single continuous profile representation rather than from independent models for each depth interval. Horizon estimates are obtained by integrating the profile representation over the specified target depths, allowing depth-specific values to emerge directly from the profile-support system. This produces a vertically coherent and internally consistent multi-output model, in which a single model can simultaneously resolve multiple horizons. Since the profile is analytically defined at each pixel, depth-specific estimates can be obtained for any location and any depth within the sampled interval.

2.3.2 Voxel profile energy

Several approaches can be used to incorporate vertical information into DSM methodologies, including spline functions and deep-learning methods. Under the ISPM framework, horizons are not independent layers but emerge from the continuous redistribution of the profile. Let the predicted voxel-scale soil property field be defined as:

$$f(v, z)$$

where v represents the spatial pixel value, which include location (x, y) and z represents depth. The function $f(v, z)$ therefore describes the predicted soil property value at every location at every depth.

The continuous soil property for the profile is calculated by integrating the voxel predictions through depth, which is a modification from gridded equal-area splines (Flynn et al., 2024):

$$F(z) = \int_0^z f(v, \tilde{z}) d\tilde{z}$$

where $F(z)$ represents the continuous soil property up to depth (z), and $\tilde{z}$ represents the depth coordinates used for transforming voxel predictions into target depth intervals. Depending on the algorithm used, $F(z)$ can represent the cumulative soil property or the mean soil property for the profile. However, this does not change the fundamental theory of ISPM.

The depth-support transformation is derived under an energy-minimisation principle, where the optimal profile configuration represents the minimum-energy redistribution of soil properties through depth. This redistribution can be interpreted through a source–sink relationship:

$$\frac{\partial E}{\partial z} = \sum Source - \sum Sink$$

where sources represent continuous soil property information entering a depth interval and sinks represent the distribution allocated to the extracted horizon or target depth interval. In this formulation, the source–sink balance is represented by the antiderivative of the depth-support function. Therefore, profile transitions continuously through depth rather than being represented as independent horizon averages.

The volumetric profile support between two depth boundaries is then calculated as:

$$\bar{V}_h = \sum_{x,y} \left[F(z_{bottom}) - F(z_{top})\right]_{x,y}$$

where $\bar{V}_h$ represents the cumulative profile energy contained within from the top of the profile (z_{top}) to the bottom (z_{bottom}).

In this study, predictions were conducted using the Random Forest algorithm (Breiman, 2001); therefore, $F(z)$ represents the weighted means of the soil property to 50 cm. To extract the distribution of soil properties at the horizon support ($\bar{h}_j$), the same formula is applied with different depth intervals:

$$\bar{h}_j = \sum_{x,y} [F(z_{max}) - F(z_1)]_{x,y} ,$$

where z_{max} is the depth of the profile and z_1 is the width of the depth interval of interest. For example, the 20-50 cm depth interval z_1 = 30 cm. Therefore, the resulting horizon estimate represents the integrated vertical redistribution of the soil property through the profile rather than a simple average of independent voxel predictions. If $F(z)$ represents the cumulative soil property, the equation is simply normalised (e.g., $z_{max} - z_1$). Importantly, the source-sink antiderivative representation equates to the original integral where the only unknown is $\tilde{z}$.

When only a limited number of sampled horizons are available, such as the two depth intervals used in Soils4Africa and iSDAsoil, the profile is only weakly constrained by observations. Consequently, the definition of $\tilde{z}$ becomes essential because it governs the redistribution of the soil property and the reconstruction of the continuous profile between the two depth intervals.

2.3.3 Depth support change

The depth-support transformation function $\tilde{z}$ must satisfy at least three conditions to conform with the ISPM framework (Flynn et al., 2026):

1. the soil property must maintain continuity through the profile,
2. singularities (e.g., zero or infinity) and boundary overlap must be avoided (e.g., $z_1 = z_{\max}$),
3. and the resulting antiderivative must contain a logarithmic term to preserve continuous mass-conservation during support redistribution.

Under these constraints, a physics-informed spline transformation (Flynn et al., 2026) was modified for a two horizon system to fulfil the requirements defined as:

$$\tilde{z} = \frac{z_1(z_{max} + z_1)}{z_{max}(z_{max} - z_1)}.$$

The transformation collapses the depth-support function into a ratio-based form in which $\tilde{z}$ becomes the only unknown support variable requiring a solution excluding the predictions. This substantially reduces computational complexity when implemented in Google Earth Engine (GEE; (Gorelick et al., 2017), while allowing continuous support redistribution across unsampled depths.

The transformation is symmetric:

$$\tilde{z}(z_1, z_{max}) = \tilde{z}(z_{max}, z_1)$$

meaning that the redistribution of soil properties is independent of the order of the input horizons. This allows the order to be reversed to account for processes such as capillary and downward movement such as leaching. The source-sink and symmetric nature generalises the framework by allowing other depth intervals to be extracted besides the original sampling intervals.

The antiderivative with respect to z_{max}, representing the structural boundary conditions controlling the redistribution term and is defined as:

$$F(z_{max}) = -z_{max} + z_1 ln \left| \frac{z_{max}}{(z_{max} - z_1)^2} \right| + C$$

This term governs the structural geometry of the properties and controls how horizon boundaries transition, while preserving continuous mass-preservation. The logarithmic component prevents singularity formation as the upper and lower depth supports approach one another, ensuring smooth redistribution across the profile.

The corresponding antiderivative with respect to z_1 represents the profile property potential extracting the sink term is:

$$F(z_1) = \frac{{z_1}^2}{2z_{max}} - 2z_1 - 2z_{max}\ln|z_{max} - z_1| + C$$

This linear-quadratic function defines how properties are redistributed between horizons. The logarithmic component controls the distribution with short depth boundaries, while the quadratic component becomes increasingly important with wider horizons.

Within this formulation, soil horizons are obtained by integrating the continuous voxel prediction field over the target depth interval. The depth transformation ($\tilde{z}$) controls the redistribution of profile support between depth boundaries, allowing horizon values to be derived from the cumulative profile integral rather than predicted as independent layers.

2.3.4 Uncertainties

Monte Carlo prediction variance was propagated through the profile-support transformation using the same integration framework as the predictions themselves rather than a delta-method approximation. This ensured that uncertainty remained independent of the predictions and facilitated direct comparison between products.

The voxel-scale variance field was defined as:

$$\sigma^2(v, z)$$

and integrated through the profile as:

$$U(z) = \int_0^z \sigma^2\,(v, \tilde{z})\,d\tilde{z}$$

where $U(z)$ represents the cumulative variance support through the profile.

The horizon-scale variance was then obtained from the support transition between depth boundaries:

$$\bar{U}_h = U(z_{\mathrm{bottom}}) - U(z_{\mathrm{top}})$$

and converted to standard deviation to maintain consistency with iSDAsoil uncertainty standards:

$$\sigma_h = \sqrt{\bar{U}_h}$$

Since cumulative variance was propagated conservatively throughout the profile, the resulting uncertainty estimates represent upper-bound or worst-case uncertainty scenarios. This was intentional to avoid artificially compressed or misleadingly low uncertainty estimates.

2.4 Evaluation

2.4.1 Spatial trends

To evaluate whether the imposed constraints improved vertical consistency across the study region, the relationship between topsoil and subsoil predictions was assessed. This was done for each soil property and soil properties on the example sites to determine any soil co-trends in the S4A predictions. A generalised additive model (GAM) was fit using residual maximum likelihood (REML) as the objective function between the topsoil and subsoil intervals, with the spatial component represented as a smooth Gaussian process:

$$y_i = f(z) + s(x, y) + \varepsilon_i$$

Where $f(z)$ represents the soil property relationship between horizons or properties, $s(x, y)$ represents the spatial surface (longitude and latitude) and ε_i represents residual variation. The ideal outcome is that the ISPM framework strengthens the intrinsic relationship between topsoil and subsoil properties while reducing the contribution of spatial autocorrelation. Under this condition, the imposed variational profile constraints would account for noise associated with heterogeneous environmental conditions across the study region. Consequently, the remaining relationship between horizons would be driven primarily by the harmonised values themselves, with only mild nonlinearity arising from pedogenic processes.

The effective degrees of freedom (edf) were used to assess the complexity of the smoothed coordinates, with values approaching one indicating an approximately linear relationship. Residual spatial autocorrelation was subsequently evaluated to determine whether spatial structure remained after accounting for both the depth-support relationship and the fitted spatial trend.

2.4.2 Evaluation metrics

Evaluation of the ISPM framework was performed on the final predictive surfaces after profile-support function into the target topsoil and subsoil intervals. Since ISPM operates on continuous voxel-scale profile fields prior to horizon extraction, evaluation statistics must be calculated on the transformed horizon predictions rather than on intermediate voxel states. A randomly 70:30 training–evaluation split was used for each soil property resulting in 1,130 training and 484 evaluation observations.

Evaluation statistics included Pearson's coefficient of determination (R^2), Lin's concordance correlation coefficient (CCC; Lin, 1989), root mean squared error (RMSE), ratio of performance to interquartile distance (RPIQ) and bias. These metrics were selected because Random Forest models typically exhibit low variance and high predictive precision (Hastie et al., 2009), attributes that can be preserved during the integration. Collectively, these statistics quantify both predictive agreement and the extent the model may introduce systematic bias between horizons.

2.5 Comparison

2.5.1 Difference in mean

A spatial Welch–Satterthwaite t-test with 10 Monte Carlo iterations (5,000 samples per iteration) was used to compare predictions from S4A and iSDAsoil over agricultural lands. Each iteration was independently resampled for each dataset, and degrees of freedom were adjusted using the Welch–Satterthwaite approximation with the nominal sample size n replaced by the effective sample size n_{eff}, accounting for spatial autocorrelation.

An assumption was made that approximately 10% of randomly sampled observations were spatially independent. While conservative, this reflects the fact that random sampling does not guarantee separation beyond the range of spatial dependence. Consequently, the effective sample size was used to reduce redundancy in the variance structure and to avoid inflation of Type I error due to spatial autocorrelation (Satterthwaite, 1946). This adjustment results in modified degrees of freedom (rather than the standard $N - 1$), providing a more realistic representation of independent information content.

2.5.2 Spatial trend

To evaluate spatial co-trends, each dataset was independently modelled as a function of spatial location fitting a GAM with the same parameters described in Section 2.4. The resulting fitted spatial trend surfaces were extracted and correlation quantified (R^2) to identify similarities in the spatial distribution between products. The correlation between S4A and iSDAsoil was conducted after fitting each surface separately to the Gaussian process smoothed coordinates.

This approach compares large-scale spatial trends rather than raw observations, thereby reducing sensitivity to fine-scale noise and spatially correlated sampling artefacts. Residual spatial autocorrelation was assessed using the residuals from the GAM model and a global Moran's I to evaluate whether remaining spatial structure persisted after smoothing.

2.6 Implementation

For clarity, the implementation of the framework was divided into three sequential components (**Fig. 2**), corresponding to each critical step taken.

A. Profile prediction

Voxel-scale profile predictions were generated using a Random Forest regression model with 100 trees and GEE's default parameters (bag fraction = 0.5, variables per split = √(number of covariates) and unlimited maximum nodes). The training dataset combined soil observations from the 0–20 cm and 20–50 cm depth intervals. This creates weighted mean profile level predictions as Random Forest takes the weighted means when multiple samples are present at the same location. Predictions were produced over agricultural areas using all 64 Google AlphaEarth (Brown et al., 2025) embeddings as covariates at a 90 m spatial resolution. Although specific regions were shown as examples due to the patchy sparse landcover data to show greater detail, statistics were conducted on the whole region. Therefore, predictions and uncertainties of S4A of the entire region can be found in **Appendix A-B** and **Appendix C-D** for topsoil and subsoil, respectively.

B. Depth-support transformation

Predicted mean profile voxel surfaces were transformed into horizon-specific depth intervals (0–20 cm and 20–50 cm) using the linear–quadratic depth-support transformation and its analytical integral formulation implemented in GEE. Once the continuous profile prediction surface was generated, $\tilde{z}$ was solved directly on the raster image to derive horizon-scale predictions. To account for uncertainty, profile prediction surfaces were generated using 10 Monte Carlo iterations, from which the mean and variance were calculated prior to solving for $\tilde{z}$. The same depth-support function was then applied to the variance surface to obtain cumulative profile variance, with standard deviation used as the uncertainty metric.

All profile-support transformations were performed directly on the raster prediction surfaces rather than at the point-observation level. While this approach enables efficient implementation within GEE, it introduces an additional computational step during post-processing of large raster datasets, which may represent a limitation for very large mapping domains.

C. Evaluation and comparison

Model outputs were evaluated separately for topsoil and subsoil horizons with two complementary comparisons being performed:

1. **Mean differences (linear comparison)**: Differences in mean values between S4A and iSDAsoil were assessed using a spatially corrected Welch's t-test.
2. **Spatial co-trend similarity (nonlinear comparison)**: Differences in spatial distributions were evaluated through a GAM fit with smoothed coordinates through a Gaussian process.

This dual approach provides both a linear assessment of the mean between products, and a nonlinear assessment of spatial pattern agreement across the landscape. The evaluation metrics were performed after the predictive surfaces were mapped and the measured data was extracted from the predictions.

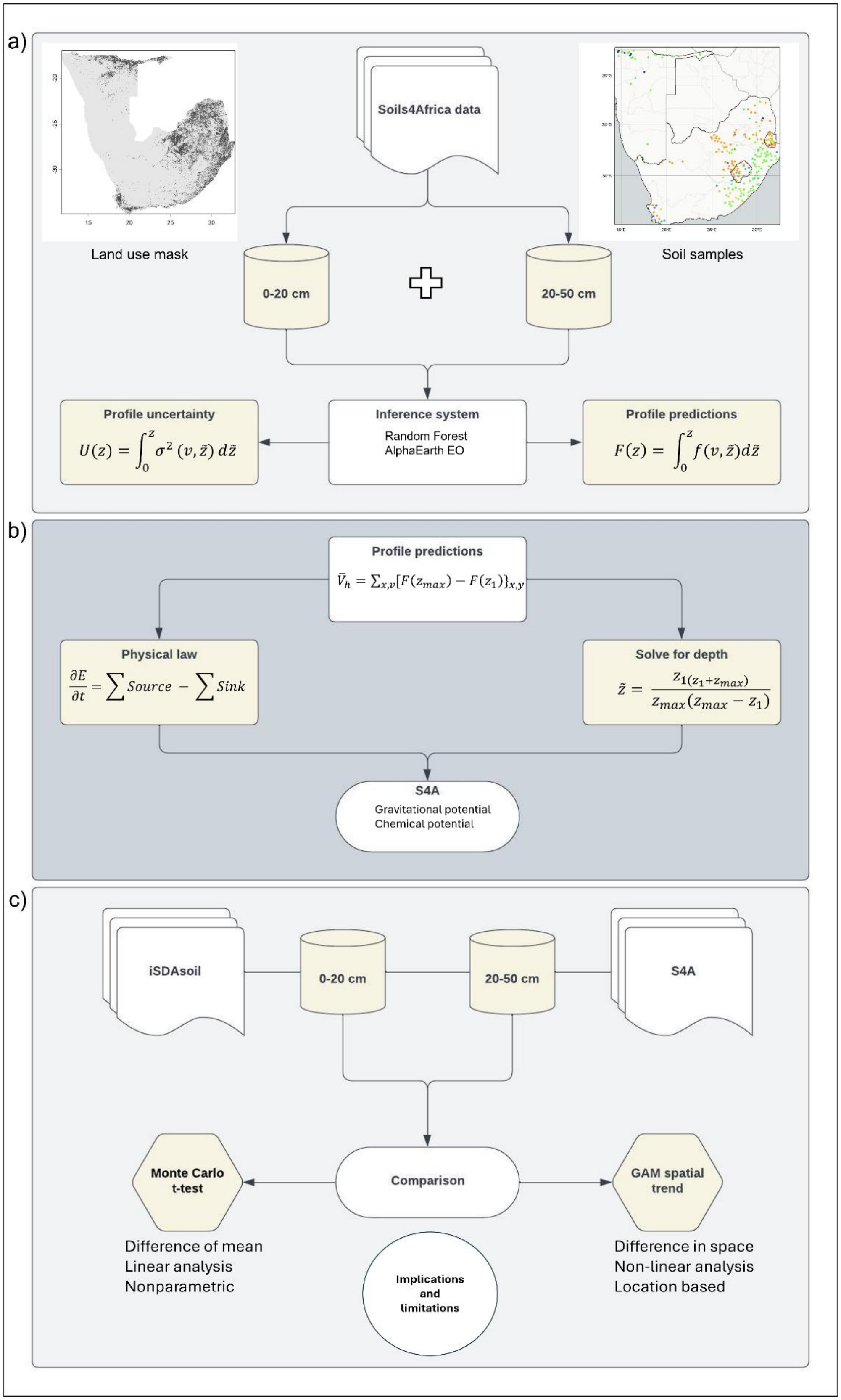

Fig. 2 *Implementation of the Integrated Soil Profile Mapping workflow, comparison with iSDAsoil and evaluation of the model*

3. Results

3.1 Summary statistics

3.1.1 Soils4Africa Prior distribution

The prior distributions of Soils4Africa soil properties were predominantly right-skewed across the study region, with clay exhibiting a bimodal structure that was more pronounced in the subsoil. Mean pH values were similar between the topsoil (6.03) and subsoil (6.09), indicating generally near-neutral conditions consistent with optimal nutrient availability for most crops. A comparable pattern was observed for cation exchange capacity (CEC), while macronutrients (N, P, K) generally exhibited mean values ranging from adequate to elevated levels, consistent with depth-dependent agricultural management.

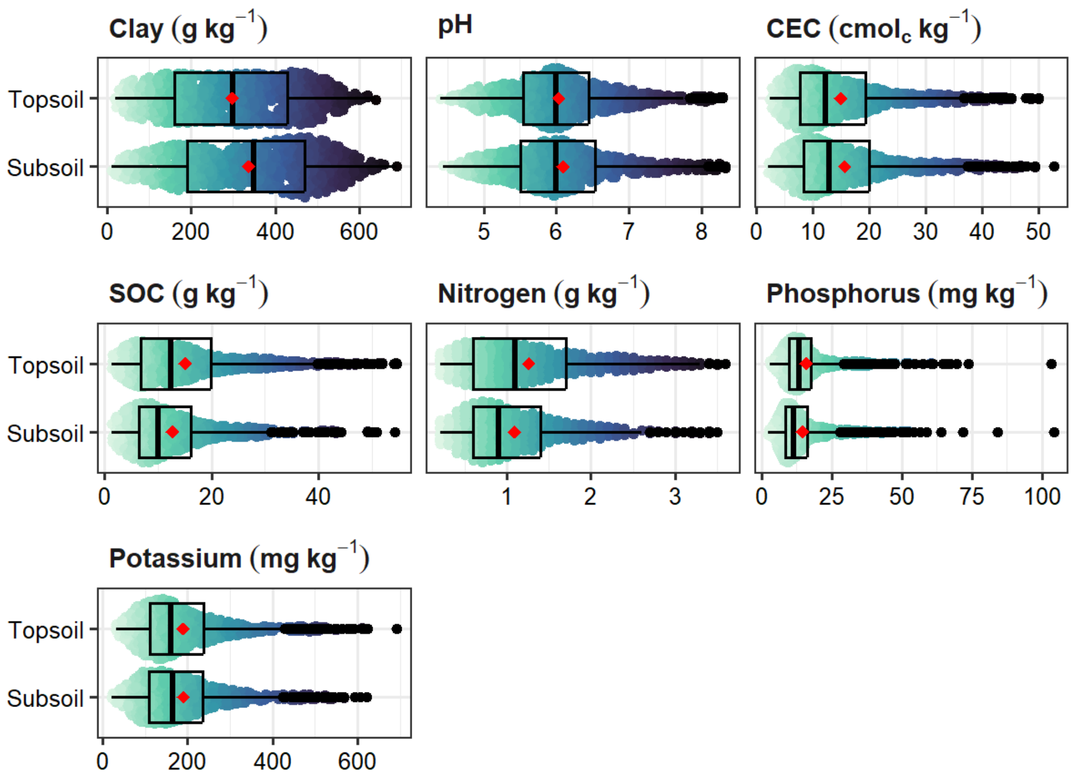

Fig. 3 *Prior data distribution of measured soil properties from Soils4Africa project on agricultural land in Namibia, South Africa, Lesotho and Eswatini*

Several other properties (notably P, SOC, and K) exhibited long-tailed distributions, suggesting potential sampling-induced variability. Phosphorus showed pronounced deviation from normality (skewness = 2.75, kurtosis = 11.7), indicating highly concentrated hotspots within the agricultural system. No prior normalisation was applied when modelling, consistent with the ISPM framework's assumption that distributional transformation is not required when vertical structure is explicitly handled through the depth-support energy formulation.

3.1.2 Posterior distributions

S4A reproduced the general depth-dependent patterns observed in Soils4Africa data. Clay, pH and CEC increased with depth, whereas SOC, N, P and K decreased, reflecting expected pedogenic and management-related gradients in agricultural soils (Figure 4). Across most properties, S4A exhibited greater variability than iSDAsoil, with the exception of pH, which showed lower dispersion in S4A. The S4A predictions also retained key characteristics of the measured data distribution, including the bimodal distribution of clay and the heavy-tailed distribution of P, whereas iSDAsoil generally produced smoother and more normally distributed outputs. A key distinction between the two products was the magnitude of depth-dependent divergence rather than a uniform offset across properties. For example, clay content differed by approximately 19%

in the topsoil and 35% in the subsoil, while similar depth-dependent differences were observed for pH, CEC, P and K.

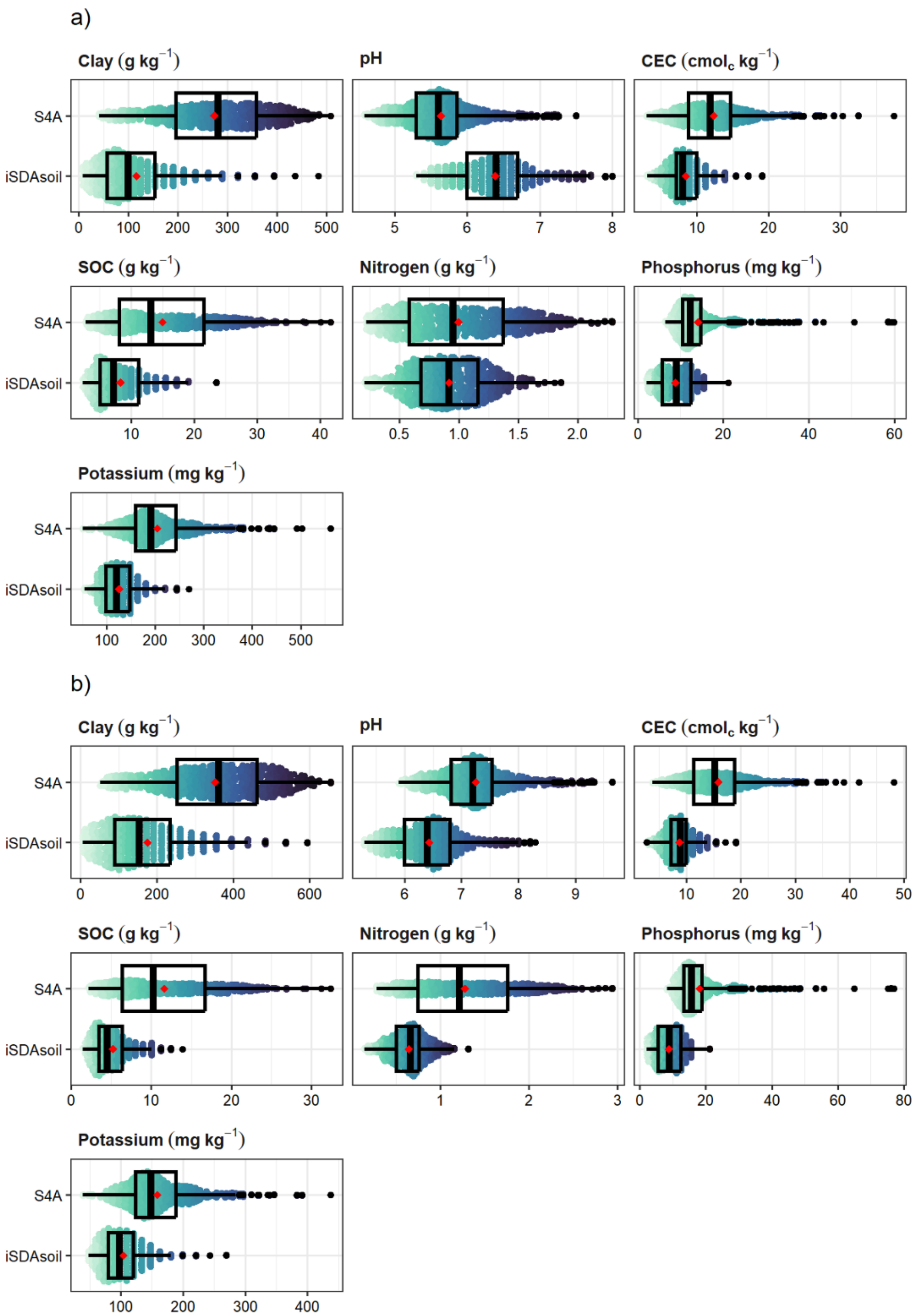

Fig. 4 *Posterior data distribution of measured soil properties from S4A model and iSDAsoil model for topsoil (a) and subsoil (b) on agricultural land in Namibia, South Africa, Lesotho and Eswatini*

In contrast, SOC and N exhibited a consistent directional separation between products, with S4A producing higher organic-related estimates across both horizons. ISPM predicted mean SOC values of 15.1 g kg^{-1} (topsoil) and 11.7 g kg^{-1} (subsoil), compared to 8.10 and 5.09 g kg^{-1} in iSDAsoil, corresponding to increases of approximately 86% and 130%, respectively. Nitrogen followed a similar but less extreme pattern with a 32% and 46% increase in the S4A data for the topsoil and subsoil, respectively.

A notable exception was pH. While both the Soils4Africa observations and iSDAsoil predictions exhibited relatively stable depth profiles, S4A showed a pronounced increase from topsoil to subsoil (5.63 to 7.24; +29%). Although this trend exceeds the central tendency observed in the measured data range (4.40–8.32), it remains physically plausible within the model constraints.

3.2 Predictions

The predictions of the full region of interest can be found in **Appendix A** through **D** for topsoil and subsoil, respectively. However, the sparse region was deemed not detailed enough to discuss in detail. Therefore, areas of high-density agricultural land were chosen to show predictions at a finer specify although all statistics were conducted on the agricultural land for all four nations.

3.2.1 Spatial trends

When analysing the trend between the properties on each site, the examples showed complex nonlinear spatial relationships with varying degrees of correlation. Clay (**Fig. 5**) and P (**Fig. 6**) showed a weak nonlinear monotonic trend with a R^2 of 0.32 (edf = 28.6, F = 178, p<0.01) in the topsoil as well as the subsoil (R^2 = 0.38, edf = 28.7, F = 182, p<0.01) with residuals having a positive spatial autocorrelation (topsoil = 0.33, subsoil 0.34) in Limpopo. On the other hand, in Eswatini, SOC (**Fig. 7**) and N (**Fig. 8**) had a strong nonlinear trend (edf = 24.3, F = 14.4, p<0.01) in the topsoil with R^2 of 0.81. The subsoil had a similar trend (edf = 24.0, F = 16.4, p <0.01) with a R^2 of 0.82 and both showed a slight positive spatial autocorrelation in the residuals (topsoil = 0.06, subsoil = 0.05, $p < 0.01$) according to the Moran's I.

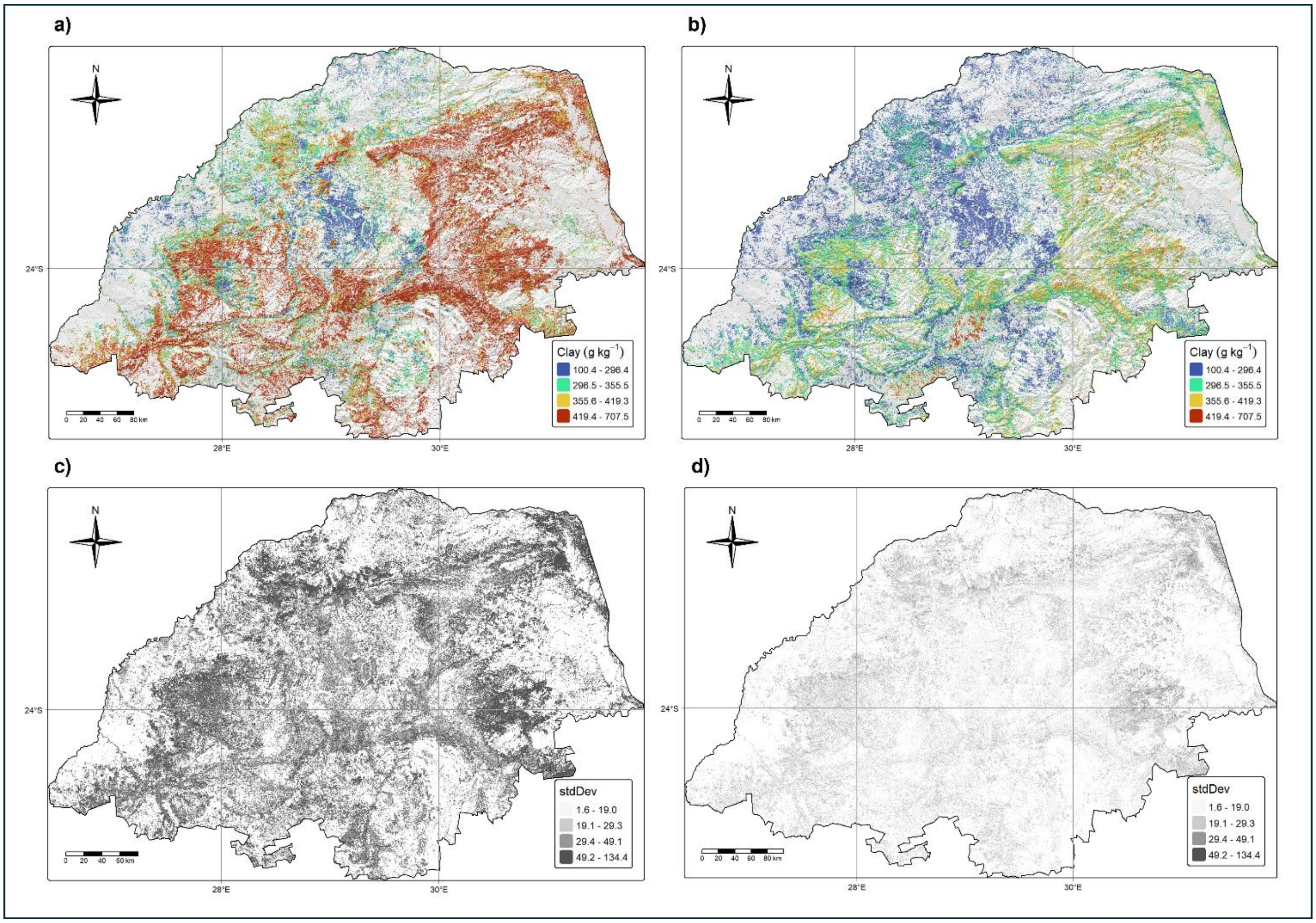

Fig. 5 *Spatial distribution of clay content in the topsoil and subsoil with standard deviation (stdDev) in Limpopo, South Africa*

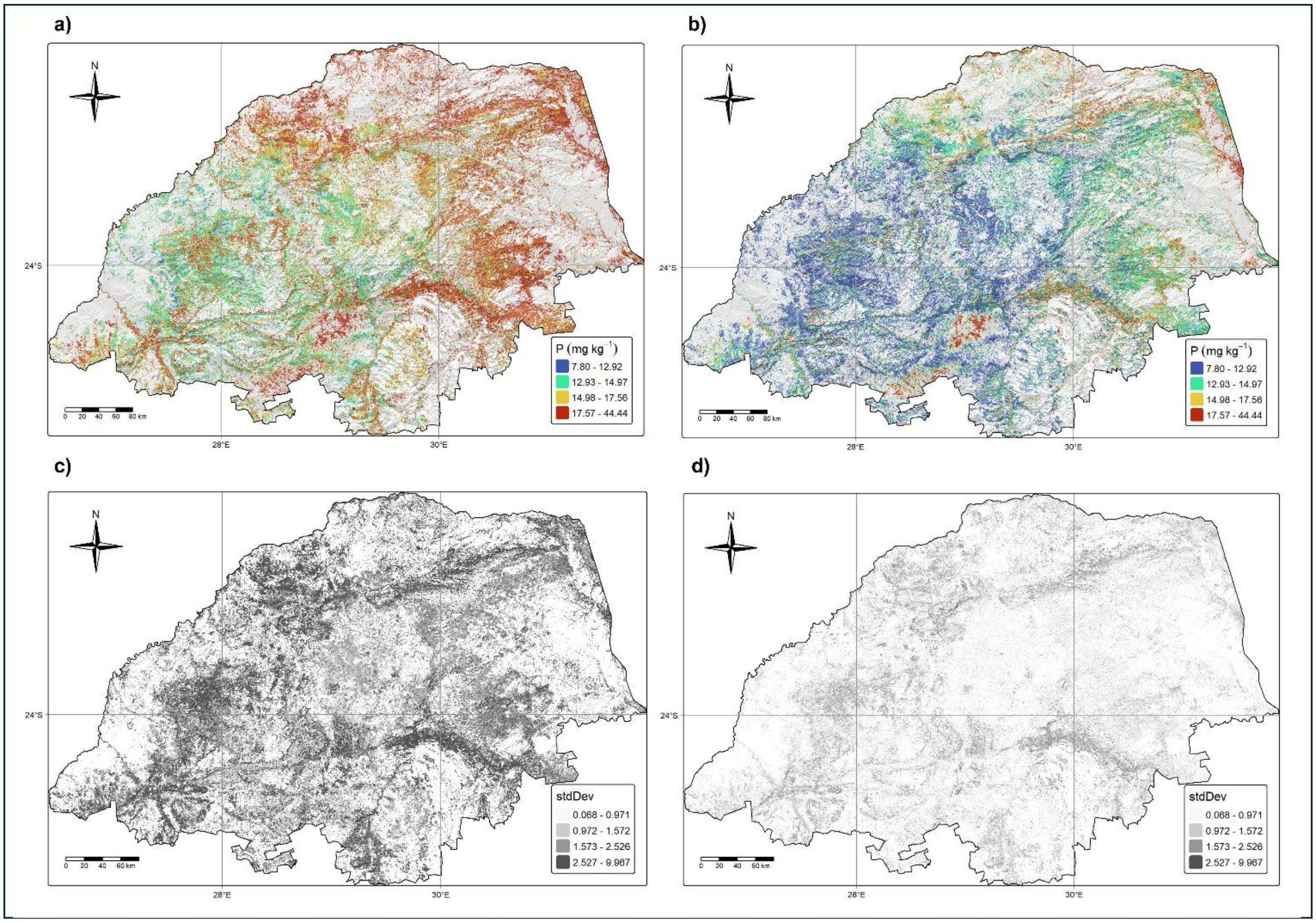

Fig. 6 *Spatial distribution of extractable phosphorus in the topsoil and subsoil with standard deviation (stdDev) in Limpopo, South Africa*

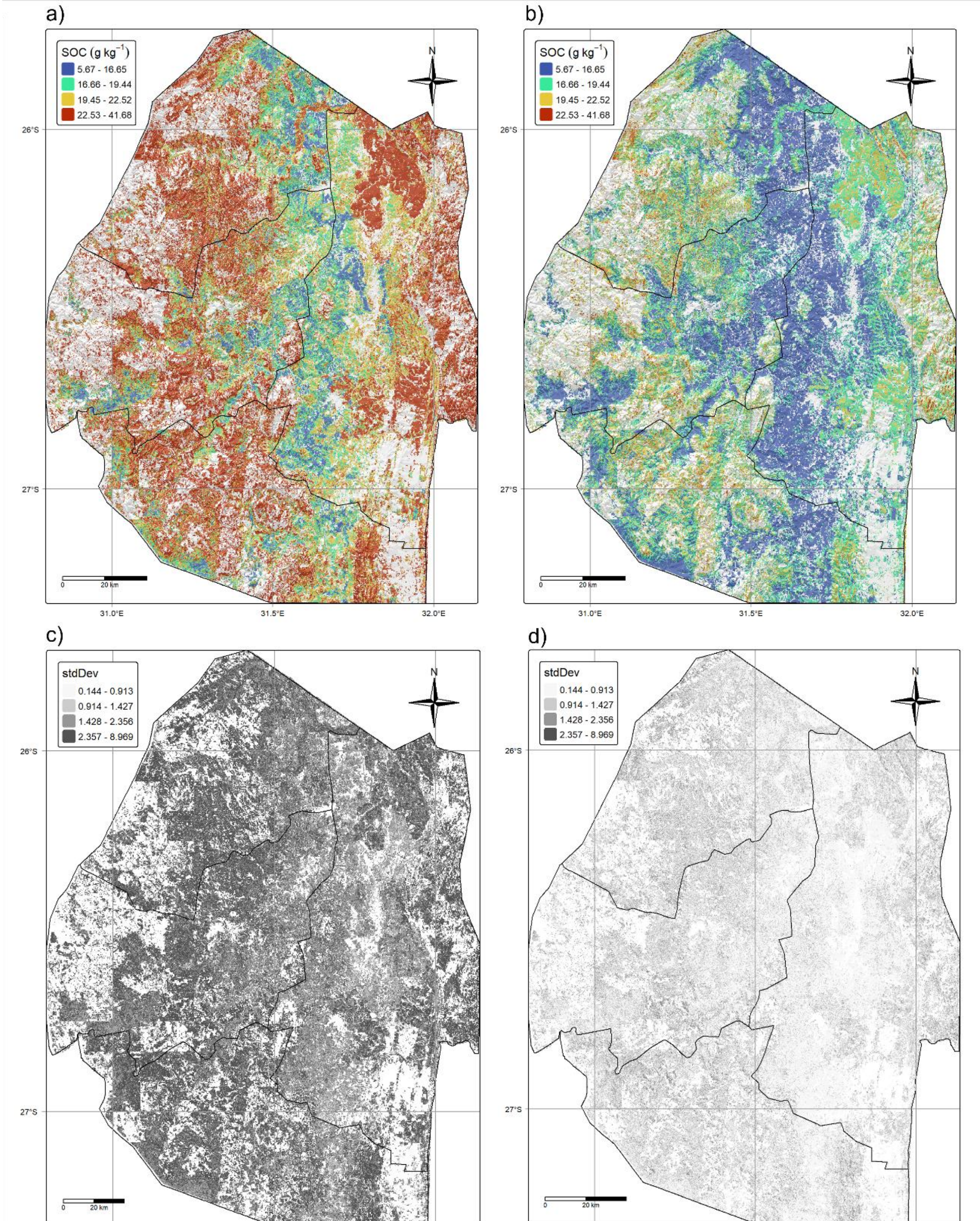

Fig. 7 *Spatial distribution of soil organic carbon content in the topsoil and subsoil with standard deviation (stdDev) in Eswatini*

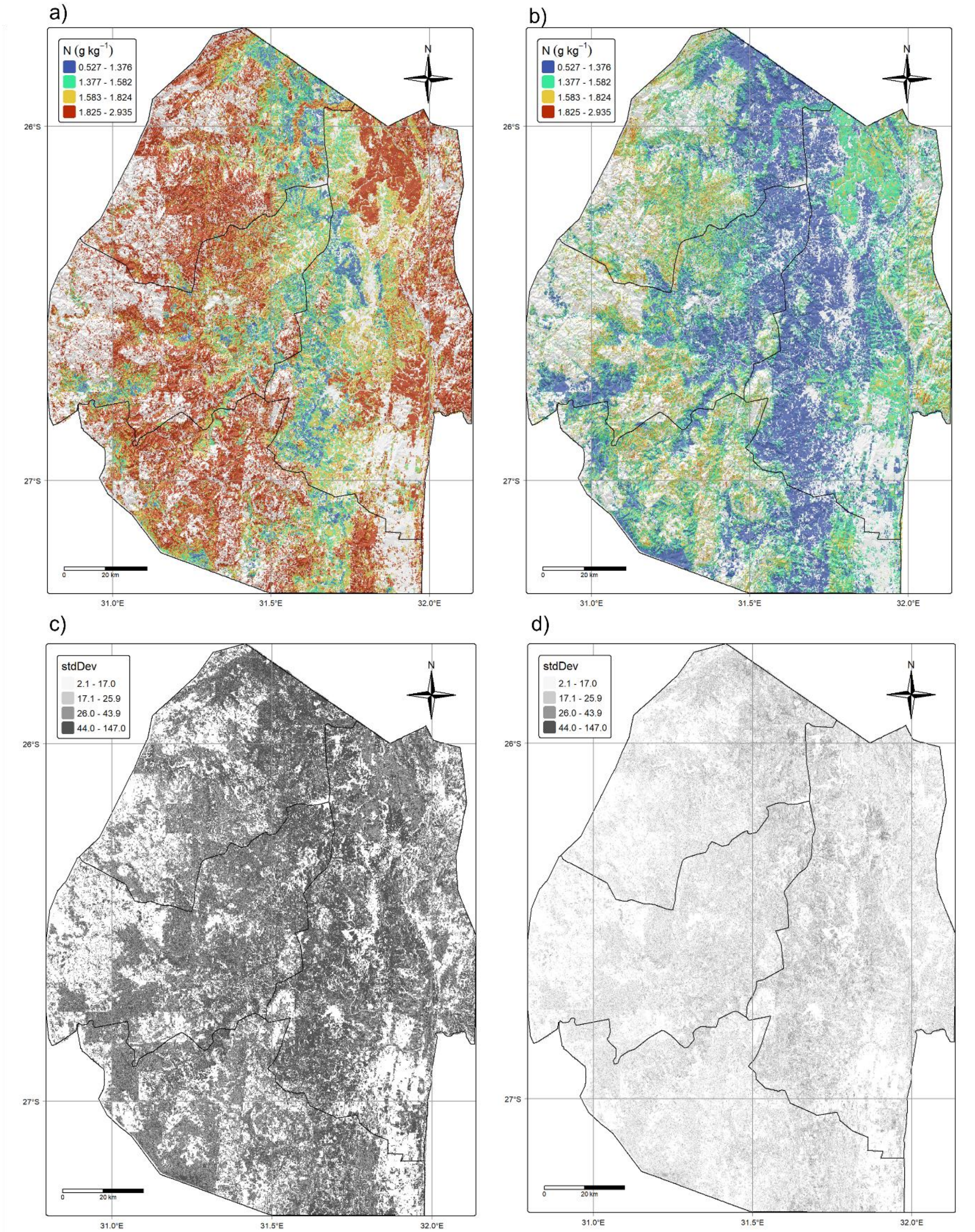

Fig. 8 *Spatial distribution of nitrogen content in the topsoil and subsoil with standard deviation (stdDev) in Eswatini*

In Kavango, K (**Fig. 9**) and CEC (**Fig. 10**) had a moderately strong nonlinear trend for both the topsoil and subsoil with a R^2 of 0.52 (edf = 27.8, F = 43.2, p<0.01) and 0.54 (edf = 27.8, F = 48.3, p<0.01), respectively. As with the other properties, the residuals had a positive spatial autocorrelation with the topsoil having a Moran's I of 0.14 and subsoil having 0.16.

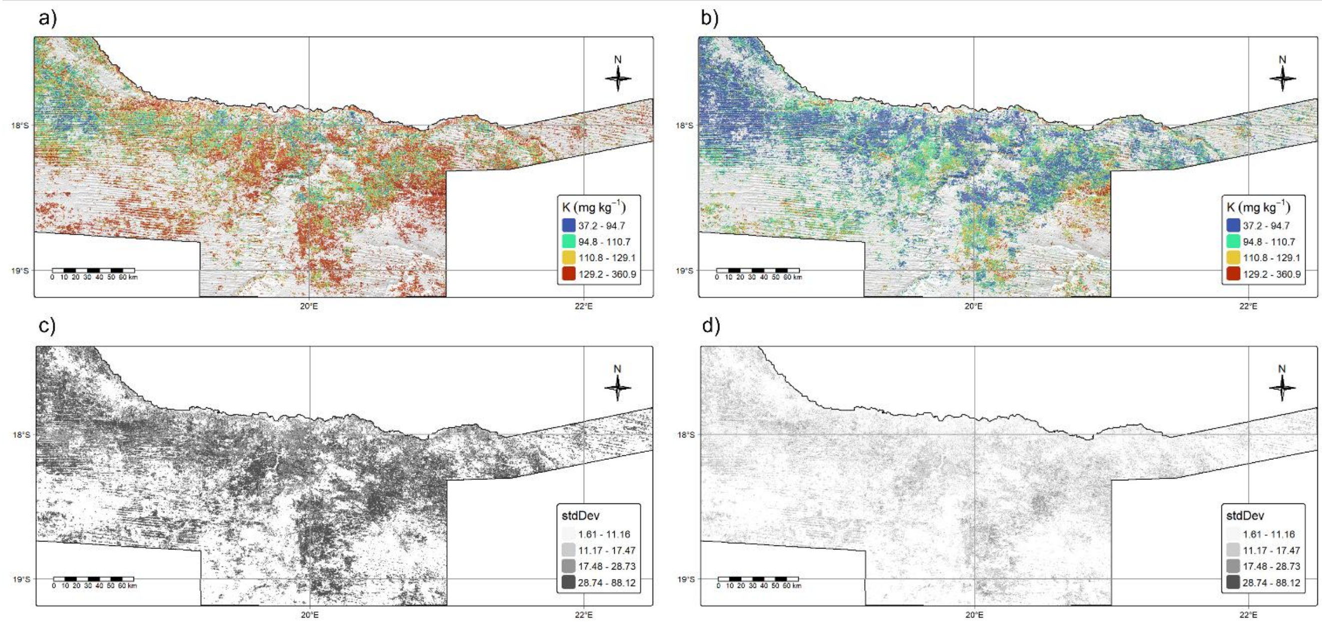

Fig. 9 *Spatial distribution of the potassium in the topsoil and subsoil with standard deviation (stdDev) in Kavango, Namibia*

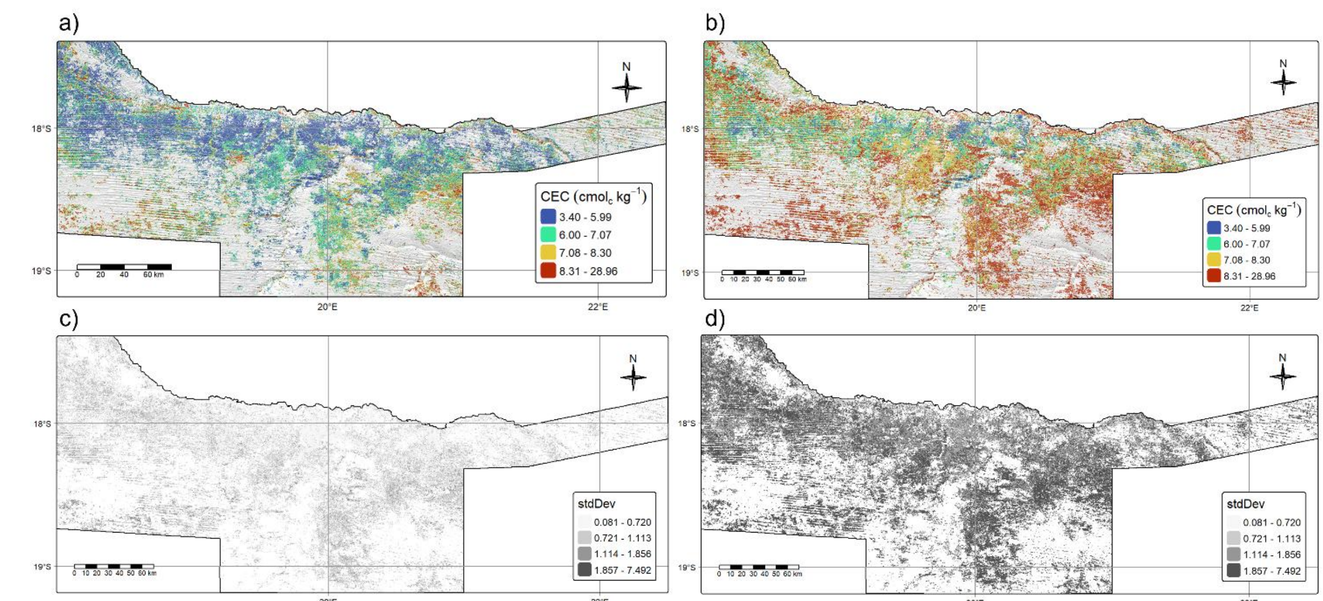

Fig. 10 *Spatial distribution of the cation exchange capacity in the topsoil and subsoil with standard deviation (stdDev) in Kavango, Namibia*

The agricultural land in Lesotho is primarily confined to the northern regions as the Drakensberg Mountain range make the terrain too steep for crop production. Along the foothills of the

Drakensberg, the soil is more acidic in the topsoil and pH drops as the elevation increases (~4.84-6.42), most likely due to an increase in precipitation (**Fig. 11**). The same trend is found in the subsoil; however, with a pH that is more suitable for crop growth (~6.23-7.41).

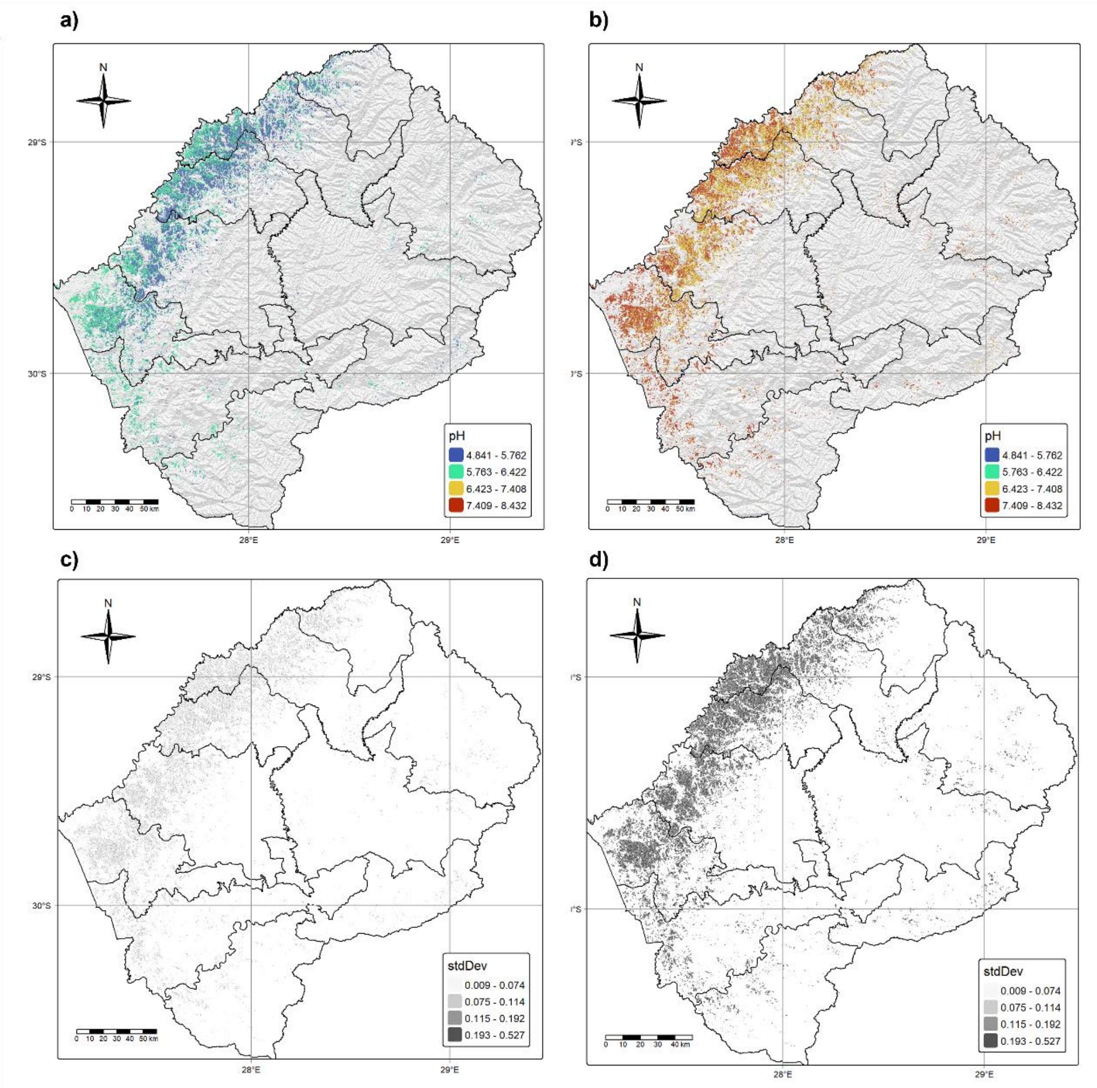

Fig. 11 *Spatial distribution of pH in the topsoil and subsoil with standard deviation (stdDev) in Lesotho*

3.2.2 Evaluation

ISPM predictions were consistently higher in performance (**Table. 2**) than models trained separately for each soil horizon, particularly for skewed variables and without prior data transformation. For example, P achieved $R^2 = 0.27$ and CCC = 0.35 (RMSE = 10.6, bias = -1.45) when predicting on the evaluation points under a baseline Random Forest topsoil model, with strongly positive residual spatial autocorrelation (Moran's *I* of = 0.77). Soil organic matter had better results with a R^2 = 0.60 and CCC = 0.72 (RMSE = 6.27, bias = 0.69) with a Moran's *I* of = 0.75. This indicates that a substantial proportion of residual structure remained correlated when predictions were made directly on point-support observations rather than area-integrated grid cells.

Table. 2 *Accuracy metrics of the S4A model giving the depth interval, R^2, Concordance correlation coefficient (CCC), root mean squared error (RMSE), Ratio of Performance to InterQuartile distance (RPIQ) and prediction bias*

Property	Depth (cm)	R^2	CCC	RMSE	RPIQ	Bias
Clay *($g\ kg^{-1}$)*	0-20	0.63	0.74	100	2.45	32.7
	20-50	0.62	0.73	101	2.57	-6.58
pH	0-20	0.76	0.72	0.40	2.09	0.04
	20-50	0.76	0.72	1.34	0.59	-1.24
CEC ($cmol_c\ kg^{-1}$)	0-20	0.74	0.76	5.07	1.19	0.33
	20-50	0.74	0.77	5.64	1.37	-3.29
SOC *($g\ kg^{-1}$)*	0-20	0.74	0.82	5.29	2.50	-1.72
	20-50	0.74	0.73	0.41	1.80	0.12
N ($g\ kg^{-1}$)	0-20	0.74	0.82	0.39	2.42	-0.16
	20-50	0.72	0.83	0.30	2.58	-0.05
P (mg kg^{-1})	0-20	0.67	0.78	7.48	0.75	-2.38
	20-50	0.66	0.72	7.65	0.57	1.79
K (mg kg^{-1})	0-20	0.72	0.75	66.3	1.16	-36.8
	20-50	0.72	0.73	61.6	0.97	9.84

In contrast, ISPM reduced residual spatial structure through the depth-support transformation while introducing horizon-dependent bias adjustments. This is reflected in the systematic divergence in bias between horizons, particularly for clay, where topsoil bias was positive (32.7 g kg^{-1}) and subsoil bias was negative (−6.58 g kg^{-1}). Similar asymmetry was observed across multiple properties, indicating that the depth-support transformation redistributes error between horizons rather than uniformly minimising it across both.

Performance metrics (RMSE, RPIQ, and bias) differed between horizons for all properties, which is consistent with the two-horizon constraint imposed by the linear–quadratic depth-support formulation in this ISPM formulation. This asymmetry was expected given that the transformation enforces a coupled vertical structure, where improvement in one horizon can partially trade off against error in the other.

Overall, CCC values ranged between 0.72 and 0.83 across properties and horizons. These values are comparable to those reported for iSDAsoil products, which report CCC values between 0.65 and 0.90 under five-fold spatial cross-validation. Although evaluation methodologies differ and are therefore not strictly equivalent, the independent evaluation dataset used in this study falls within the reported performance envelope of iSDAsoil for all evaluated properties. Additional metrics (e.g., CCC and RPIQ) were not reported for iSDAsoil, limiting direct metric-by-metric comparison. However, given the overlap in R^2 ranges and the consistency of evaluation data distributions, the ISPM results were considered comparable within the constraints of cross-study evaluation uncertainty.

The energy-minimisation formulation produced a distinct separation between spatial structure and vertical dependency in the topsoil–subsoil relationship (**Table. 3**). Across the full study region, ISPM-derived relationships between horizons were well correlated ($R^2 \approx 0.99$), with only weak and statistically non-significant nonlinearity ($p > 0.01$), indicating that residual variation was largely decoupled from spatial structure. Or in other words, the correlation came from the values themselves without any spatial autocorrelation.

Table. 3 *Correlation between topsoil and subsoil in the S4A dataset, correlation of the raw Soils4Africa data, the effective degrees of freedom (edf), F-statistic and p-value (p<0.01)*

	R^2(S4A)	R^2 (Soils4Africa)	edf	F-statistic	p-value
Clay *(g kg^{1})*	0.99	0.80	3.19	0.54	0.72
pH	0.99	0.87	2.10	1.51	0.21
CEC *(cmol$_c$ kg^{-1})*	0.99	0.82	5.64	2.56	0.01
SOC *(g kg^{1})*	0.99	0.81	2.40	0.40	0.75
N *(g kg^{1})*	0.99	0.81	3.30	0.83	0.52
P *(mg kg^{1})*	0.99	0.62	2.32	1.02	0.35
K *(mg kg^{1})*	0.99	0.77	2.05	0.20	0.83

In contrast, the raw data exhibited strong nonlinear dependence between topsoil and subsoil values, with R^2 values ranging from 0.62 to 0.87 across soil properties. Generalised additive model (GAM) decomposition showed that spatial structure accounted for a substantial proportion of the observed deviance, with effective degrees of freedom (edf) ranging from 2.34 (K) to 18.71 (pH), explaining approximately 62%–92% of total variation. After application of ISPM, spatial structure was substantially reduced, with the residuals of the GAM showing comparatively lower complexity (edf ≈ 2.10–5.64) and no statistically significant spatial dependence (p > 0.01).

Relative to the raw Soils4Africa data, ISPM increased the strength of the topsoil–subsoil relationship by approximately 15%–61% for skewed properties. Across soil properties, the expected theoretical depth ratios derived from the transformation ($\tilde{z}$) converged toward characteristic scaling factors of approximately 1.2 for properties increasing with depth and 0.8 for properties decreasing with depth. The empirical ratios obtained from model outputs were 1.28 and 0.78 respectively, indicating close agreement with the theoretical depth-support formulation, although not fully converged to the optimal energy-minimising state.

3.3 Comparison

3.3.1 Difference in mean

Spatial Welch–Satterthwaite t-tests indicated that only topsoil nitrogen (N) exhibited statistically similar means between S4A and iSDA ($p > 0.01$), highlighting relative agreement for this property despite differences in spatial support between continental-scale modelling and agricultural-land-focused sampling (**Table. 4**). However, the effect sizes (Cohen's *d*) revealed systematic differences between datasets that varied by soil property and depth.

Table. 4 *Spatial Welch's-Satterthwaite t-test approximation with Cohen's d effect size, T-statistic, degrees of freedom (df) and statistical significance (p-value > 0.01)*

	Effect size	T-statistic	df	p-value
Clay *(g kg^{1})*	0.52	42.0	443	<0.01
	0.95	42.5	412	0.00
pH	-1.96	-26.8	368	0.00
	1.11	-25.5	415	0.00
CEC *(cmol$_{c}$ kg^{-1})*	1.48	14.3	326	0.00
	2.06	20.4	352	0.00
SOC *(g kg^{-1})*	1.10	10.9	352	0.00
	1.42	14.5	355	0.00

N ($g\ kg^{-1}$)	0.05	0.43	272	0.67
	1.41	14.5	354	0.00
P (mg kg^{-1})	2.55	28.3	401	0.00
	2.34	25.7	432	0.00
K (mg kg^{-1})	2.00	22.2	408	0.00
	1.85	17.3	290	0.00

The smallest magnitudes of difference were observed for clay (topsoil: 0.52; subsoil: 0.95), consistent with the relatively stable and slowly varying nature of texture-related properties. Total N also showed comparatively low effect sizes (topsoil: 0.05; subsoil: 1.41). In contrast, P exhibited the largest divergence between products, with effect sizes of 2.55 (topsoil) and 2.34 (subsoil). CEC and SOC showed intermediate to high effect sizes.

pH exhibited a directional inconsistency across horizons, with a large negative effect size in the topsoil (−1.96), indicating lower mean values in S4A relative to iSDAsoil, while subsoil values showed the opposite directional behaviour (1.11). This aligns with expected sensitivity of chemical properties to differences in sampling support, spatial coverage and model formulation between S4A and iSDAsoil products.

3.3.2 Spatial trends

Despite statistically significant differences in mean values between S4A and iSDA, both products exhibited strong nonlinear agreement in spatial structure, indicating that a substantial proportion of inter-product variability is driven by shared spatial autocorrelation rather than independent signal divergence. For pH, strong spatial co-structure was observed, with high agreement in both the topsoil ($R^2 = 0.87$) and subsoil ($R^2 = 0.99$). These values indicate that both products reproduce nearly identical spatial gradients, although differences in magnitude persist. It is important to note that this metric reflects similarity in spatial pattern rather than equality in absolute values.

CEC exhibited similarly strong spatial agreement, with $R^2 = 0.76$ in the topsoil and $R^2 = 0.99$ in the subsoil, indicating increasingly convergent spatial structure with depth. SOC showed consistently high spatial correspondence, with $R^2 = 0.95$ in the topsoil and $R^2 = 0.92$ in the subsoil, making it the most spatially stable property across depths in terms of cross-product structural agreement. Nitrogen also exhibited strong spatial alignment, with $R^2 = 0.85$ in the topsoil and near-perfect agreement in the subsoil ($R^2 \approx 0.99$). Notably, this contrasts with the mean-based comparison, where topsoil N was the only property without a statistically significant difference in mean values, while subsoil N did showed a significant difference. This suggests that spatial structure is preserved even when marginal distributions diverge between datasets. Phosphorus displayed comparatively weaker spatial agreement in the topsoil ($R^2 = 0.60$) but stronger correspondence in the subsoil ($R^2 = 0.86$), consistent with higher spatial heterogeneity and sensitivity to land management effects.

Although S4A incorporated Google AlphaEarth embeddings as covariates, the resulting spatial patterns closely align with those represented in iSDAsoil, suggesting that both modelling frameworks capture similar large-scale environmental gradients despite differences in model structure and training data. Consequently, the observed spatial agreement is consistent with expectations that dominant pedo-evironmental controls are shared across both products, even where absolute magnitudes differ.

4. Discussion

Soils4Africa data was used to implement a novel DSM approach in which horizon values were derived from voxel-scale profile predictions through an antiderivative-based depth-support transformation. This introduces vertical constraints and enables coherent back-transformation to target depth intervals. The resulting S4A product was compared with the continental-scale iSDAsoil dataset to assess differences in predicted soil properties across agricultural land and to evaluate potential changes since the most recent continental mapping effort.

4.1 Predictions

Although the measured Soils4Africa dataset exhibited strong positive skewness typical of nutrient distributions in agricultural systems (Arumugam et al., 2025), the bimodal distribution observed for clay was consistent with fixed-depth sampling rather than strict horizon sampling. From a pedometric perspective, this highlights a limitation of non-horizon sampling designs, where heterogeneous soil property distributions within depth intervals may induce distributions difficult to model. This has implications for subsequent harmonisation procedures, which are typically applied post hoc (e.g., equal-area splines or phySplines), but may decrease vertical gradients or introduce instability in proportional representations when horizons are modelled independently.

Nevertheless, model performance was not substantially affected by the skewed distributions, likely because the vertical constraints reduced the number of feasible profile configurations and acted as a regularising mechanism on the solution space. Furthermore, the prior and posterior distributions followed similar patterns between Soils4Africa observations and S4A prediction surfaces, indicating that ISPM largely preserved the measured data distribution without requiring transformation of the response variables. The framework also substantially linearised the relationship between topsoil and subsoil properties, suggesting that the predominant vertical structure of the soil system follows a relatively stable scaling relationship despite considerable local and regional heterogeneity. However, this result was expected as the topsoil and subsoil were extracted from the same predictions and integral.

In addition, ISPM reduced residual spatial autocorrelation across the landscape between horizons. When horizons were modelled independently without constraints, a substantial proportion of explained variance was due to spatial autocorrelation rather than the predicted values. In contrast, the ISPM transformation reduced spatial dependence in the residuals. The reduction in variability across both inter-horizon and intra-horizon scales suggests that a portion of the apparent noise arose from unresolved depth processes rather than purely spatial processes. The depth-support therefore not only stabilised relationships between topsoil and subsoil intervals but also reduced variability within horizons themselves through mass-preservation and voxel-scale integration.

As expected, both SOC and N had a decreasing trend with depth in Eswatini and were highly correlated with one another. They highlands had higher values of both values relative to the semi-arid savannah biome of central Eswatini, with the same trend in uncertainties. This is a common trend in the country with the climatic and vegetation gradient. Although total N was measured, mineralisation of soil organic matter produces inorganic N through microbially mediated oxidation pathways (Daly et al., 2021). Nitrogen cycling in managed agricultural systems is also strongly linked to microbial C dynamics through coupled C–N feedback mechanisms (Li et al., 2025). Consequently, the observed relationship between SOC and N likely reflects shared microbial and vegetation regulation of organic matter turnover and nutrient mineralisation (Farzadfar et al., 2021).

Although clay and P spatial distribution in Limpopo followed a similar trend with increased values in highlands such as the Soutpansberg and Waterberg Mountains, clay and P exhibited relatively weak association in Limpopo. This likely reflects contrasting vertical distributions within the profile, where sandy topsoil has reduced P sorption capacity, while clay-enriched subsoil increases sorption potential (Simpson et al., 2025). Additionally, semi-arid savannah systems generally support lower organic matter accumulation, limiting the formation of stable organo-phosphorus complexes that would otherwise strengthen coupling between clay and P dynamics (McLaren et al., 2015).

Unlike the other soil properties, CEC and K did not follow similar spatial distributions in Kavango but showed and inverse relationship similar to clay and P in Limpopo. Although the underlying mechanisms differ, this pattern likely reflects the influence of fertiliser inputs and other surface-driven routes. Under normal conditions, K would be expected to accumulate where CEC is greater, particularly in subsoil horizons with weathering of minerals such as orthoclase (K-feldspar) (Li et al., 2016). However, the predominantly Arenosols (sandy soil) of Kavango generally possess low CEC throughout the profile, reducing their ability to retain exchangeable K (Strohbach and Petersen, 2007). Consequently, K may be susceptible to downward leaching beyond 50 cm depth or removal from the profile following fertiliser application and seasonal summer rainfall events, resulting in residual K accumulation in the topsoil.

The agricultural lands in Lesotho were generally confined to the lowlands or foothill zones of the northern Drakensberg Mountains. The pH is very acidic in the topsoil with a low of 4.81, indicating high rainfall with leaching or ammonium fertiliser use. This indicates challenges for agriculture with a decrease in labile P and micronutrients with leaching of macronutrients. There is also a possibility of Al toxicity. However, the subsoil is much more alkaline ranging from 6.42 to 8.32 indicating pH only leached to the 20-50 cm depth interval or the shape depth-support transformation was had the wrong shape despite the adequate accuracy. When inspecting the prior distribution, it was assumed the latter and the depth-support shape most likely needs adjustment.

4.2 Comparison

The posterior distributions differed substantially between products, with S4A retaining the strong positive skewness observed in the original data, whereas iSDAsoil exhibited a more normally distributed response. This difference is likely attributable to differences in modelling frameworks. ISPM employed a dimensional transformation, while preserving the original response variable distribution, whereas iSDAsoil reflects differences in data processing, algorithm or response variable transformations used during model development. However, this does not directly imply the reason iSDAsoil had a more normal posterior distribution.

With the exception of topsoil pH, S4A produced higher values than iSDAsoil. This shows evidence of a changing soil condition between iSDAsoil's inception and Soils4Africa measurements. The effect size of most soil properties was more than one standard deviation higher in S4A than iSDAsoil indicating CEC, SOC, N, P and K have all increased. An SOC was most likely due to sustainable practices such as no-till, minimal till, crop rotation or rotational grazing that has become widely adapted (Beillouin et al., 2022; Mangole et al., 2025), while N, P and K could come from sustainable fertiliser such as manure and crop residues (El-Sayed, 2020). However, the decrease in pH of the topsoil suggests that an increase in ammonium based fertiliser was the predominant source (Wang et al., 2020).

A possible increase in the soil condition in these four Southern African countries is especially important due to an increase in drought and floods (Meque et al., 2026). Therefore, the use of sustainable land management practices, largely driven by regional policies, have implications for food security. For example, in partnership with The Department of Forestry, Fisheries and the Environment and the Department of Agriculture and the International Union for Conservation of Nature, Limpopo is implementing its own regional policy on land degradation in drought prone regions (DFFE and IUCN, 2021).

On a broad scale, The Southern African Development Community (SADC) has many sustainable land management and environmental projects such as the SADC Great Green Wall Initiative and Protocol on Environmental Management for Sustainable Development to mitigate desertification and support national conservation agriculture policy (SADC Secretariat, 2025). Due to these initiatives, soil resilience and food security in these countries may be improving. Hence, the increase in effect size relative to iSDAsoil. Not surprisingly, according to the models, these initiatives have affected the topsoil more than the subsoil in their relative spatial trend.

The stronger spatial agreement observed in the subsoil suggests that the 0–20 cm layer has undergone greater anthropogenic modification since the development period represented within the observations of iSDAsoil. Nevertheless, the 20–50 cm interval remains within the active rooting and disturbance depth of major regional cropping systems such as maize, indicating that anthropogenic influence likely extended throughout much of the modelled profile (Ordóñez et al., 2018). This could explain the high correlation throughout the profile, and the sustainable practices influence to at least 50 cm in depth.

Soil organic carbon exhibited strong agreement in spatial trends between products, with high co-trend coefficients in both the topsoil (0.95) and subsoil (0.92). The effect size was greater in the subsoil (1.42) than in the topsoil (1.10), indicating larger differences in the magnitude of predicted SOC at depth, while maintaining similar spatial patterns. This was encouraging because the spatial distribution of SOC was largely consistent despite differences in absolute values. Given the importance of SOC for soil fertility, aggregate stability, water-holding capacity, biodiversity and the mitigation of land degradation (Trivedi et al., 2018), the strong agreement in spatial trends suggests that both products identify similar regions of relative C enrichment. Continued regional initiatives and research efforts focused on improving SOC management may contribute to the consistent increase in SOC with depth.

The similarity in topsoil N means between products was unexpected given the little convergence observed for other nutrients. However, N fertiliser is typically prioritised in agricultural management relative to P and K inputs, potentially contributing to greater temporal stability in mean N levels across the region. Nevertheless, due to the C-N microbial-mediated feedbacks discussed in Section 4.1, N can be tightly coupled with C and therefore, showed a similar trend in effect size and spatial distribution. The weaker topsoil spatial trend for N was interpreted as having a comparatively higher mobility than subsoil. Ammonium (NH_4^+) is rapidly mineralised to nitrate (NO_3^-) during nitrification (Yang et al., 2026), substantially increasing movement through the soil profile (Jury and Nielsen, 1989). This likely contributed to the stronger spatial agreement observed in the subsoil horizon, where redistribution processes integrate N over broader spatial scales and coincide with shifts in other properties such as pH, which can influence the form of N at these depths due to microbial manipulation (Zhou et al., 2019).

In contrast, P and K were more strongly constrained by mineral interactions and surface processes. Phosphorus is readily sorbed onto mineral surfaces, while K retention is strongly influenced by CEC and climate (Wu et al., 2025). Both nutrients are therefore more susceptible to redistribution through erosion and surface management processes within the 0-20 cm layer. Although having a lower concentration, the NPK distributions become comparatively more stable with depth, consistent with the stronger subsoil spatial agreement observed between S4A and iSDAsoil. Besides fertiliser, increased liming may have increased the labile P content in S4A; however, this hypothesis is not supported by the pH values. Nevertheless, in some areas such as Lesotho it may improve agriculture potential. Additionally, it is unclear whether an increase in these soil properties represents an increase in soil condition or simply anthropogenic additions.

4.3 Limitations

The agricultural land-use mask would benefit from additional non-agricultural exclusions such as national parks, protected game reserves and expanded urban boundaries. However, accurate land-use classification within arid and semi-arid savannah ecosystems remains challenging because these landscapes are characterised by high spatial heterogeneity, uneven mixtures of woody and herbaceous vegetation, strong seasonal variability, dormancy and diverse land-management practices (Kaszta et al., 2016).

At present, the predictive framework is more reliable at broad regional scales than for fine management zones. At a 90 m resolution, agricultural areas often appeared highly patchy and locally inconsistent. In some cases, apparent agricultural classifications occurred within strongly urbanised environments such as Johannesburg or on steep slopes within the Drakensberg where cultivation is unlikely. Consequently, mapping at continental-to-regional scales becomes difficult without a hierarchical or dashboard-style visualisation (e.g., GEE) capable of contextualising local management zones.

Improvements could involve broadening the agricultural mask to reduce isolated patches, while simultaneously strengthening exclusion criteria for non-agricultural land. Alternatively, increasing spatial resolution to better match the scale of fragmented management zones may improve representation, although this would require substantially denser sampling support and computational power.

The use of a spatial Welch's t-test for comparison across a large and environmentally heterogeneous region could be a limitation. Although mean-based comparisons provide a straightforward and relatively unbiased summary for sparse datasets, complex soil systems cannot be fully characterised through a single statistical metric (Fraixedas et al., 2022; Marshall et al., 2020). While the additional spatial trend analysis partially addresses this limitation by evaluating agreement in spatial structure, a more comprehensive comparison would require multivariate or bivariate spatial decision-support approaches capable of identifying synergistic and divergent regions between products (Cobos et al., 2024).

Differences between source datasets likely helped contribute to the observed divergence in means between S4A and iSDAsoil. The Soils4Africa dataset used for the S4A model consisted of a temporally consistent sampling campaign collected within 2023 in this region and was restricted to agricultural land. However, sample density remained low (approximately 1,614 samples; ~0.001

samples per km^{-2}), which can contribute to higher uncertainties and some soil-forming factors may not be adequately captured (Hartemink et al., 2008).

In contrast, iSDAsoil incorporated substantially larger sample density (>70,000 observations; ~0.004 samples per km^{-2}) across continental Africa, but the data originated from multiple datasets collected over inconsistent time periods and sampling protocols (Miller et al., 2021). Consequently, differences in temporal consistency, sampling density and spatial support likely contributed to the observed differences in mean values despite strong agreement in spatial trends. For this reason, no direct accuracy reassessment of iSDAsoil was performed on Soils4Africa data, as such comparison would likely reflect dataset structure rather than true model superiority.

4.4 Implications

From a computational perspective, ISPM provides an efficient approach for continental-scale soil mapping. Spatially explicit methods such as regression kriging, Gaussian process models and deep learning approaches can become computationally intensive when applied across large regions with increasing spatial resolution, environmental covariates, and training datasets (Hengl et al., 2017). In contrast, ISPM introduces a deterministic depth-support transformation that efficiently incorporates vertical profile constraints and is suitable for implementation within scalable cloud-computing environments.

The consistent topsoil–subsoil relationships observed following transformation suggest that soil profiles may exhibit transferable vertical scaling behaviour across broad geographic regions, although these relationships remain dependent on depth representation, sampling support and landscape heterogeneity. This highlights a fundamental challenge in DSM, where soil observations represent discrete samples of continuous depth functions influenced by sampling support, measurement scale and depth discretisation (Malone et al., 2009; Minasny and McBratney, 2016). Approaches such as equal-area splines and related depth-function models were developed to address these challenges by providing consistent estimates of soil properties across standardised depth intervals (Bishop et al., 1999; Malone et al., 2009; Bishop et al., 2015).

More broadly, ISPM provides an intermediate approach between purely empirical DSM and mechanistic soil modelling by constraining statistical predictions according to pedologically meaningful profile structures. This creates opportunities for harmonising heterogeneous soil datasets within a common framework while reducing artefacts associated with independent depth predictions, including unrealistic discontinuities between adjacent soil layers (McBratney et al., 2003).

Future research should evaluate ISPM using denser depth-resolved observations, alternative depth-support formulations and further advancing analytically solvable challenges. Importantly, future development should prioritise integration and updating of existing soil information resources rather than continued generation of independent products. Developing continuously updated soil information systems provides a mechanism for maintaining consistent, timely and decision-relevant soil information for environmental monitoring and agricultural management (Arrouays et al., 2014; Hengl et al., 2017; Poggio et al., 2021). An updated pan-African soil information system could therefore strengthen long-term monitoring of soil condition under changing environmental conditions (Mesele et al., 2026).

5. Conclusion

This study introduced Integrated Soil Profile Mapping, a profile-informed digital soil mapping framework that incorporates vertical soil-profile constraints directly into prediction through an energy-minimisation approach. By representing soil profiles as continuous depth-resolved soil system, the framework integrates prediction and depth harmonisation while maintaining spatial variability across heterogeneous soil landscapes. Integrated Soil Profile Mapping produced coherent vertical estimates, reduced residual spatial autocorrelation and provided stable predictions across variably landscapes and climates.

Comparison with the iSDAsoil product showed broadly consistent regional spatial patterns, while differences in predicted soil properties revealed substantial spatial variation in soil condition across Southern African agricultural lands. In particular, the results indicated variable increases in all properties measured and a decline in topsoil pH, highlighting contrasting trajectories in soil fertility and chemical condition. These patterns are consistent with differences in agricultural management and intervention, but may also reflect regional variation in climate, soil characteristics and management history; therefore, causal attribution requires further investigation.

Overall, Integrated Soil Profile Mapping provides a framework for generating internally consistent, depth-resolved soil information while retaining the vertical structure of soil profiles. Its application to emerging continental soil datasets provides a basis for more systematic assessment of regional soil condition and environmental change. Future integration and assimilation of complementary soil datasets could support continuously updated pan-African soil information systems, strengthening soil monitoring, sustainable agricultural management, soil resilience assessment and food-security planning.

Appendix A: topsoil estimates

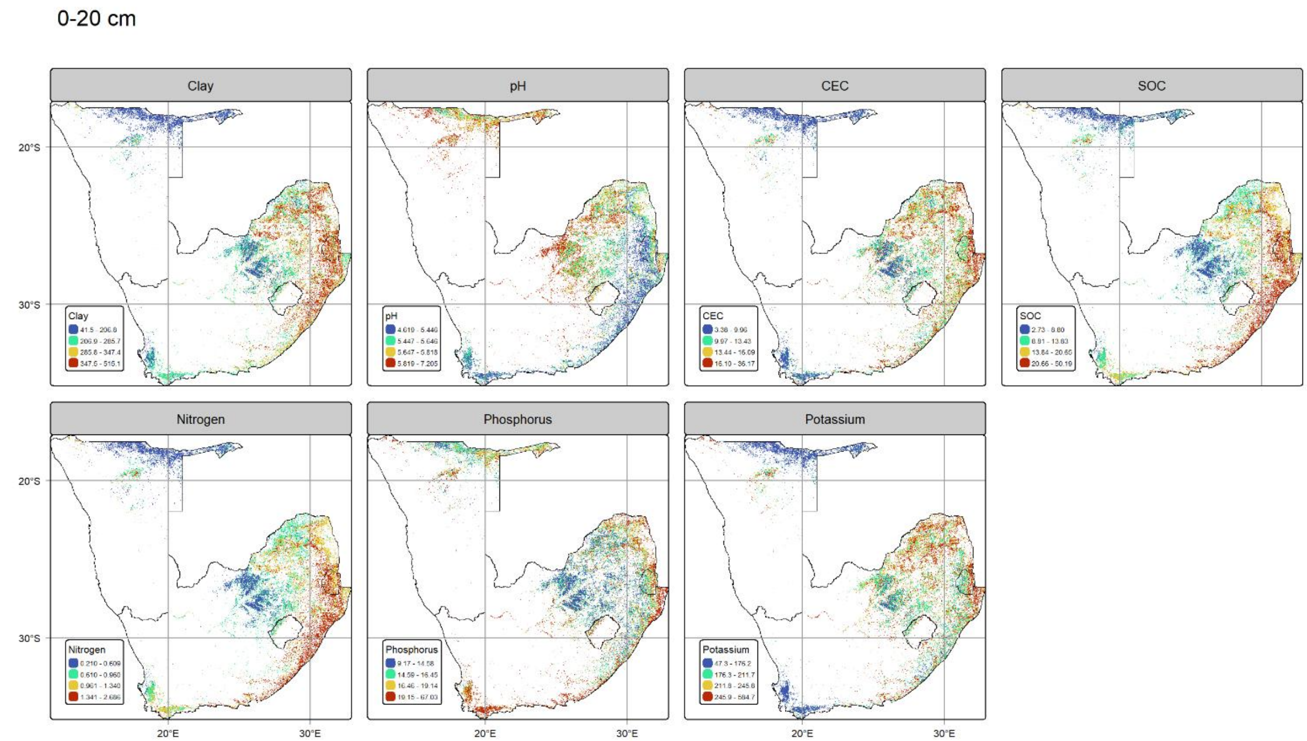

Appendix. A *All of the topsoil property estimates for Namibia, South Africa, Lesotho and Eswatini encompassing the agricultural lands delineated in the Soils4Africa project*

Appendix B: topsoil standard deviation

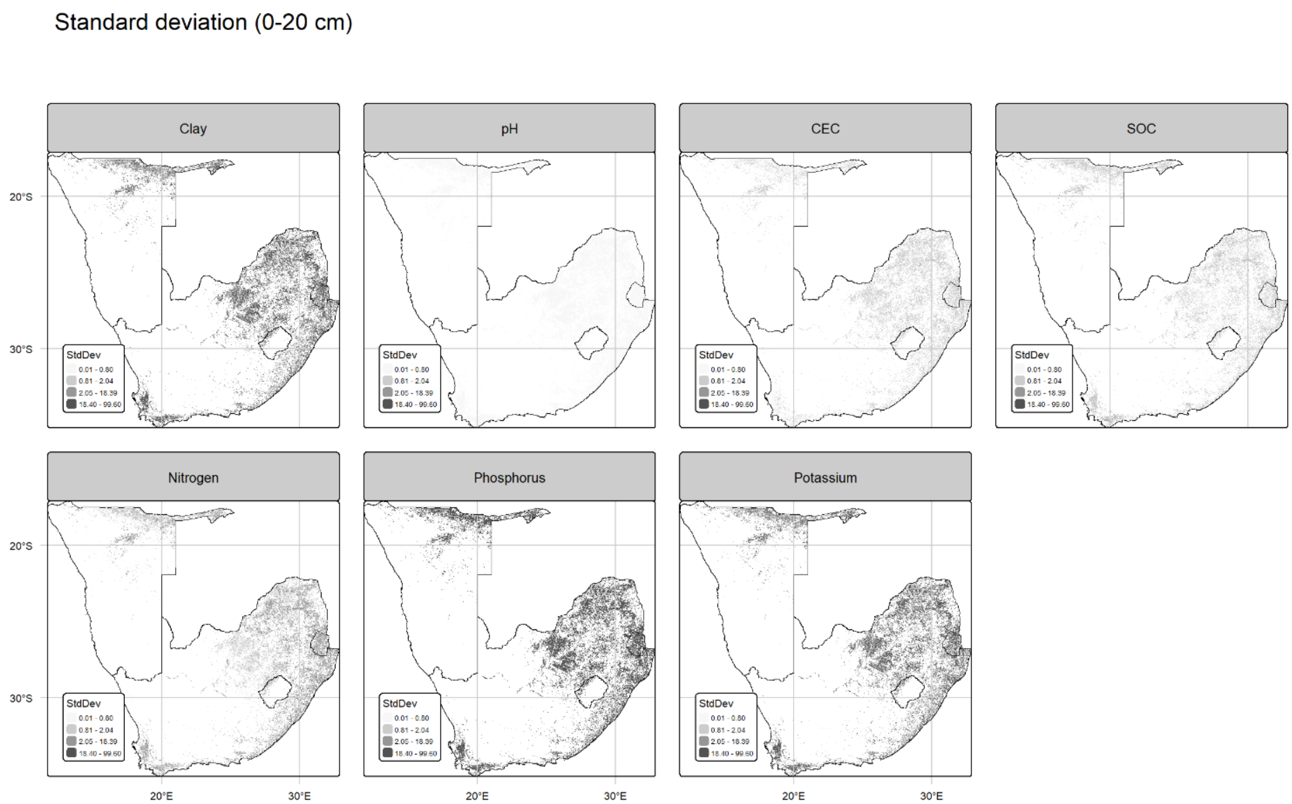

Appendix. B *All of the topsoil property standard deviation estimates (stdDev) for Namibia, South Africa, Lesotho and Eswatini encompassing the agricultural lands delineated in the Soils4Africa project*

Appendix C: subsoil estimates

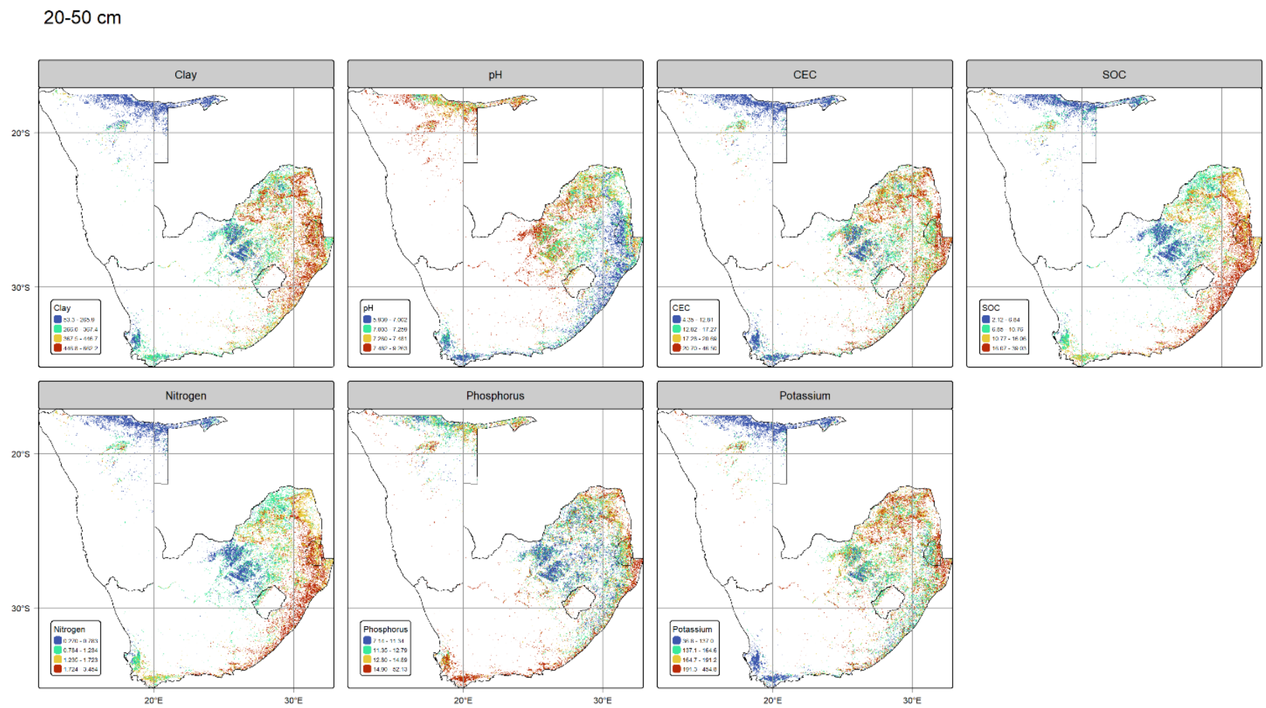

Appendix. C *All of the subsoil property estimates for Namibia, South Africa, Lesotho and Eswatini encompassing the agricultural lands delineated in the Soils4Africa project*

Appendix D: subsoil standard deviation

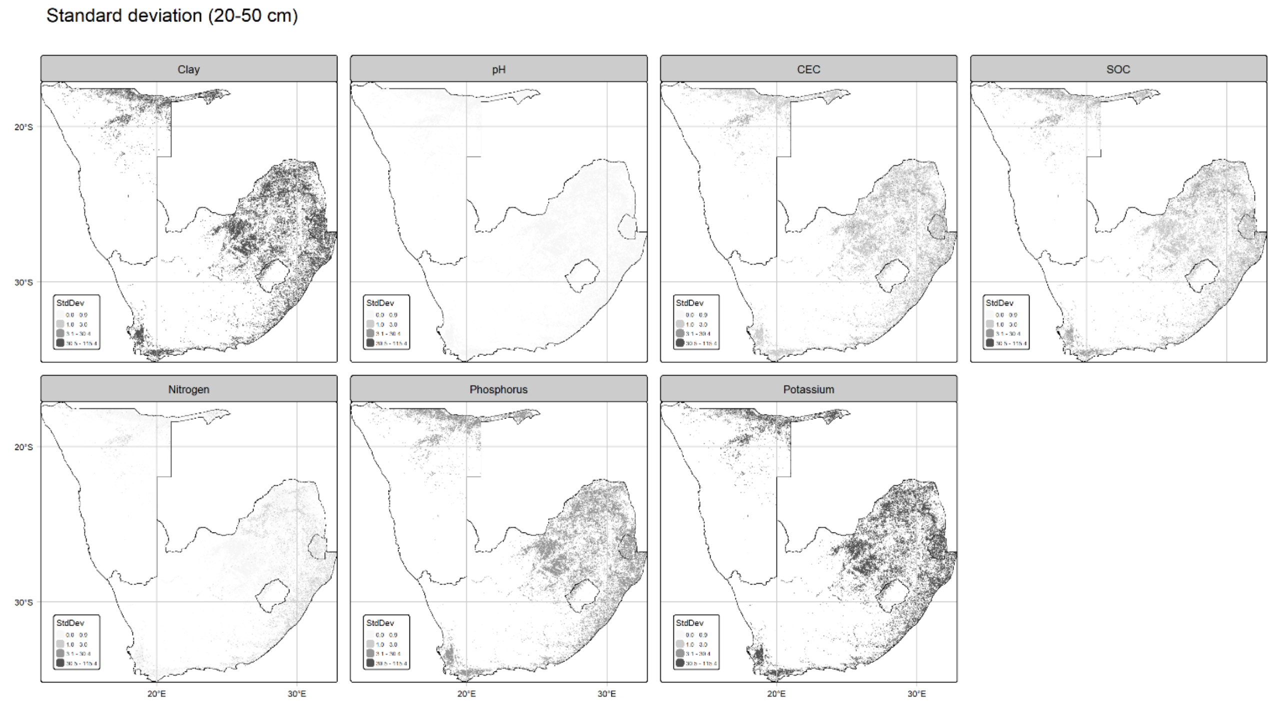

Appendix D *All of the subsoil property standard deviation (stdDev) estimates for Namibia, South Africa, Lesotho and Eswatini encompassing the agricultural lands delineated in the Soils4Africa project*

Funding

The research was funded by the EU Horizon 2020 Research and Innovation Programme under Grant Agreement 869200, Soils4Africa project.

Acknowledgments

The authors appreciate the contributions of the various soil surveyors who collected soil samples and conducted field assessments under harsh environmental and logistical conditions.

References

Arrouays, D., McKenzie, N., Hempel, J., Richer de Forges, A., McBratney, A., 2014. GlobalSoilMap: Basis of the global spatial soil information system, in: Arrouays, D., McKenzie, N., Hempel, J., Richer de Forges, A., McBratney, A.B. (Eds.), . Presented at the 1st GlobalSoilMap Conference, CRC Press, Orleans, France.

Arumugam, T., Kinattinkara, S., Vellingiri, K., Arumugam, M., Rajamani, J., Jayaseelan, A., 2025. Assessment of agricultural soil quality in macro and micronutrient analysis of Kasargod, Kerala, India, using GIS techniques. Journal of Hazardous Materials Advances 19, 100846. https://doi.org/10.1016/j.hazadv.2025.100846

Ballin, Barcaroli, G., Masselli, M., 2023. Calibration in LUCAS 2018 survey: 2023 edition. European Commission: Eurostat, LU. https://doi.org/10.2785/238299

Beillouin, D., Demenois, J., Cardinael, R., Berre, D., Corbeels, M., Fallot, A., Boyer, A., Feder, F., 2022. A global database of land management, land-use change and climate change effects on soil organic carbon. Sci Data 9, 228. https://doi.org/10.1038/s41597-022-01318-1

Bishop, T.F.A., McBratney, A.B., Laslett, G.M., 1999. Modeling soil attribute depth functions with equal-area quadratic smoothing splines. Geoderma 91, 27–45. https://doi.org/10.1016/S0016-7061(99)00003-8

Breiman, L., 2001. Random Forests (No. 9788578110796). Berkeley, California. https://doi.org/10.1017/CBO9781107415324.004

Brown, C.F., Kazmierski, M.R., Pasquarella, V.J., Rucklidge, W.J., Samsikova, M., Zhang, C., Shelhamer, E., Lahera, E., Wiles, O., Ilyushchenko, S., Gorelick, N., Zhang, L.L., Alj, S., Schechter, E., Askay, S., Guinan, O., Moore, R., Boukouvalas, A., Kohli, P., 2025. AlphaEarth Foundations: An embedding field model for accurate and efficient global mapping from sparse label data. https://doi.org/10.48550/arXiv.2507.22291

Cobos, M.E., Owens, H.L., Soberón, J., Peterson, A.T., 2024. Detailed multivariate comparisons of environments with mobility oriented parity. biogeography 17, e132916. https://doi.org/10.21425/fob.17.132916

Daly, A.B., Jilling, A., Bowles, T.M., Buchkowski, R.W., Frey, S.D., Kallenbach, C.M., Keiluweit, M., Mooshammer, M., Schimel, J.P., Grandy, A.S., 2021. A holistic framework integrating plant-microbe-mineral regulation of soil bioavailable nitrogen. Biogeochemistry 154, 211–229. https://doi.org/10.1007/s10533-021-00793-9

Dewitte, O., Jones, A., Spaargaren, O., Breuning-Madsen, H., Brossard, M., Dampha, A., Deckers, J., Gallali, T., Hallett, S., Jones, R., Kilasara, M., Le Roux, P., Michéli, E., Montanarella, L., Thiombiano, L., Van Ranst, E., Yemefack, M., Zougmore, R., 2013. Harmonisation of the soil map of Africa at the continental scale. Geoderma 211–212, 138–153. https://doi.org/10.1016/j.geoderma.2013.07.007

DFFE, IUCN, 2021. MAINSTREAMING SUSTAINABLE LAND MANAGEMENT (SLM) FOR LARGE-SCALE IMPACT IN THE GRAZING LANDS OF LIMPOPO AND NORTHERN CAPE PROVINCES IN SOUTH AFRICA: ENVIRONMENTAL AND SOCIAL MANAGEMENT FRAMEWORK (ESMF) (No. GEF ID 10179).

El-Sayed, A.-F.M., 2020. Semi-intensive culture, in: Tilapia Culture. Elsevier, pp. 69–101. https://doi.org/10.1016/B978-0-12-816509-6.00005-7

Farzadfar, S., Knight, J.D., Congreves, K.A., 2021. Soil organic nitrogen: an overlooked but potentially significant contribution to crop nutrition. Plant Soil 462, 7–23. https://doi.org/10.1007/s11104-021-04860-w

Flynn, T., Kostecki, R., Rebi, A., Raza, T., 2024. Accessing global soil raster images and equal-area splines to estimate soil organic carbon stocks on the regional scale. Pedosphere S1002016024000699. https://doi.org/10.1016/j.pedsph.2024.07.004

Flynn, T., Rasaei, Z., Kostecki, R., 2026. Smoothing Earth's surface: The complexity of soil texture class transitions. Science of The Total Environment 1025, 181621. https://doi.org/10.1016/j.scitotenv.2026.181621

Fraixedas, S., Roslin, T., Antão, L.H., Pöyry, J., Laine, A.-L., 2022. Nationally reported metrics can't adequately guide transformative change in biodiversity policy. Proc. Natl. Acad. Sci. U.S.A. 119, e2117299119. https://doi.org/10.1073/pnas.2117299119

Gorelick, N., Hancher, M., Dixon, M., Ilyushchenko, S., Thau, D., Moore, R., 2017. Google Earth Engine: Planetary-scale geospatial analysis for everyone. Remote Sensing of Environment 202, 18–27. https://doi.org/10.1016/j.rse.2017.06.031

Hartemink, A.E., McBratney, A.B., Mendonça-Santos, M. de L. (Eds.), 2008. Digital soil mapping with limited data. Springer, Dordrecht ; London.

Hastie, T., Tibshirani, R., Friedman, J., 2009. The Elements of Statistical Learning, 2nd ed. Springer Series in Statistics.

Hengl, T., Mendes De Jesus, J., Heuvelink, G.B.M., Ruiperez Gonzalez, M., Kilibarda, M., Blagotić, A., Shangguan, W., Wright, M.N., Geng, X., Bauer-Marschallinger, B., Guevara, M.A., Vargas, R., MacMillan, R.A., Batjes, N.H., Leenaars, J.G.B., Ribeiro, E., Wheeler, I., Mantel, S., Kempen, B., 2017. SoilGrids250m: Global gridded soil information based on machine learning. PLoS ONE 12, e0169748. https://doi.org/10.1371/journal.pone.0169748

Huising, J.E., Mesele, S.A., 2022. Protocol for field survey: guidelines for field surveyors on soil sample collection and field assessment of agricultural lands in Africa. IITA, Ibadan, Nigeria. https://doi.org/https://hdl.handle.net/10568/139527

Jury, W.A., Nielsen, D.R., 1989. Nitrate Transport and Leaching Mechanisms, in: Developments in Agricultural and Managed Forest Ecology. Elsevier, pp. 139–157. https://doi.org/10.1016/B978-0-444-87393-4.50011-3

Kaszta, Ż., Van De Kerchove, R., Ramoelo, A., Cho, M., Madonsela, S., Mathieu, R., Wolff, E., 2016. Seasonal Separation of African Savanna Components Using Worldview-2 Imagery: A Comparison of Pixel- and Object-Based Approaches and Selected Classification Algorithms. Remote Sensing 8, 763. https://doi.org/10.3390/rs8090763

Kempen, B., Brus, D., de Sousa, L., 2021. Soils4Africa Sampling Design. ISRIC, Wageningen, The Netherlands.

Kempen, B., Brus, D.J., Stoorvogel, J.J., 2011. Three-dimensional mapping of soil organic matter content using soil type–specific depth functions. Geoderma 162, 107–123. https://doi.org/10.1016/j.geoderma.2011.01.010

Leenaars, J.G.B., Van Oostrum, A.J.M., Ruiperez Gonzalez, M., 2014. Africa Soil Profiles Database Version 1.2 A compilation of georeferenced and standardised legacy soil profile data for Sub-Saharan Africa (with dataset).

Li, T., Wang, H., Zhou, Z., Chen, X., Zhou, J., 2016. A new grading system for plant-available potassium using exhaustive cropping techniques combined with chemical analyses of soils. Sci Rep 6, 37327. https://doi.org/10.1038/srep37327

Li, W., Wang, G., Mu, Z., Qi, S., Zhou, S., Xiang, D., 2025. Microbially-Mediated Soil Carbon-Nitrogen Dynamics in Response to Future Soil Moisture Change. Earth’s Future 13, e2024EF005521. https://doi.org/10.1029/2024EF005521

Lin, L.I.-K., 1989. A concordance correlation coefficient to evaluate reproducibility. Biometrics 45, 255–268.

Ma, Y., Minasny, B., McBratney, A., Poggio, L., Fajardo, M., 2021. Predicting soil properties in 3D: Should depth be a covariate? Geoderma 383, 114794. https://doi.org/10.1016/j.geoderma.2020.114794

Malone, B.P., McBratney, A.B., Minasny, B., Laslett, G.M., 2009. Mapping continuous depth functions of soil carbon storage and available water capacity. Geoderma 154, 138–152. https://doi.org/10.1016/j.geoderma.2009.10.007

Mangole, C.D., Maina, C.M., Mulungu, K., Tschopp, M., Harari, N., Suresh, R., Kassie, M., 2025. Adoption of sustainable land and water management practices and their impact on crop productivity among smallholder farmers in sub-Saharan Africa. Land Use Policy 153, 107533. https://doi.org/10.1016/j.landusepol.2025.107533

Marshall, E., Wintle, B.A., Southwell, D., Kujala, H., 2020. What are we measuring? A review of metrics used to describe biodiversity in offsets exchanges. Biological Conservation 241, 108250. https://doi.org/10.1016/j.biocon.2019.108250

McBratney, A.B., Santos, M.L.M., Minasnya, B., 2003. On digital soil mapping. Geoderma 117, 3–52. https://doi.org/10.1016/S0016-7061(03)00223-4

McLaren, T.I., Smernik, R.J., McLaughlin, M.J., McBeath, T.M., Kirby, J.K., Simpson, R.J., Guppy, C.N., Doolette, A.L., Richardson, A.E., 2015. Complex Forms of Soil Organic Phosphorus–A Major Component of Soil Phosphorus. Environ. Sci. Technol. 49, 13238–13245. https://doi.org/10.1021/acs.est.5b02948

Meque, A.O., Richard, Y., Odoulami, R.C., Pinto, I.S., 2026. Seasonal Drought Persistence Over Southern Africa and Four of Its Major River Basins. Intl Journal of Climatology 46, e70392. https://doi.org/10.1002/joc.70392

Mesele, S.A., Csorba, Á., Kempen, B., Steverink-Mosugu, M., Babatunde, A.B., Ouessar, M., Rozanov, A., Yameogo, P.L., Traore, M., Okoti, M., Michéli, E., Huising, E.J., 2026. A Continental-Scale Framework for Harmonised Soil Monitoring in African Agricultural Lands: Design, Implementation, and Baseline Field Observations from the Soils4Africa Project. Soil Systems 10, 79. https://doi.org/10.3390/soilsystems10070079

Miller, M.A.E., Shepherd, K.D., Kisitu, B., Collinson, J., 2021. iSDAsoil: The first continent-scale soil property map at 30 m resolution provides a soil information revolution for Africa. PLOS Biology 19, e3001441–e3001441. https://doi.org/10.1371/journal.pbio.3001441

Minasny, B., McBratney, A.B., 2016. Digital soil mapping: A brief history and some lessons. Geoderma 264, 301–311. https://doi.org/10.1016/j.geoderma.2015.07.017

Mucina, L., Rutherford, M.C. (Eds.), 2024. Zonal biomes of southern Africa, Biome ecology. Springer, Cham.

Ordóñez, R.A., Castellano, M.J., Hatfield, J.L., Helmers, M.J., Licht, M.A., Liebman, M., Dietzel, R., Martinez-Feria, R., Iqbal, J., Puntel, L.A., Córdova, S.C., Togliatti, K., Wright, E.E., Archontoulis, S.V., 2018. Maize and soybean root front velocity and maximum depth in Iowa, USA. Field Crops Research 215, 122–131. https://doi.org/10.1016/j.fcr.2017.09.003

Poggio, L., De Sousa, L.M., Batjes, N.H., Heuvelink, G.B.M., Kempen, B., Ribeiro, E., Rossiter, D., 2021. SoilGrids 2.0: Producing soil information for the globe with quantified spatial uncertainty. SOIL 7, 217–240. https://doi.org/10.5194/soil-7-217-2021

Ponce-Hernandez, R., Marriott, F.H.C., Beckett, P.H.T., 1986. An improved method for reconstructing a soil profile from analyses of a small number of samples. Journal of Soil Science 37, 455–467.

SADC Secretariat, 2025. SADC ESIA and SEA Guidelines 2025. SADC Secretariat, Gaborone.

Satterthwaite, F.E., 1946. An Approximate Distribution of Estimates of Variance Components. Biometrics Bulletin 2, 110. https://doi.org/10.2307/3002019

Sharififar, A., McBratney, A., Minasny, B., 2026. Depth-resolved mapping of soil temperature in Australia using mechanistic and machine-learning approaches. Geoderma 471, 117863. https://doi.org/10.1016/j.geoderma.2026.117863

Simpson, Z.P., Mott, J., Elkin, K., Buda, A., Faulkner, J., Hapeman, C., McCarty, G., Foroughi, M., Hively, W.D., King, K., Osterholz, W., Penn, C., Williams, M., Witthaus, L., Locke, M., Pawlowski, E., Dalzell, B., Feyereisen, G., Dolph, C., Bjorneberg, D., Nouwakpo, K., Rogers, C.W., Scott, I., Bolster, C.H., Duriancik, L., Kleinman, P.J.A., 2025. Phosphorus lability across diverse agricultural contexts with legacy sources. J of Env Quality 54, 851–869. https://doi.org/10.1002/jeq2.20632

Strohbach, B.J., Petersen, A., 2007. Vegetation of the central Kavango woodlands in Namibia: An example from the Mile 46 Livestock Development Centre. South African Journal of Botany 73, 391–401. https://doi.org/10.1016/j.sajb.2007.03.002

Trivedi, P., Singh, B.P., Singh, B.K., 2018. Soil Carbon, in: Soil Carbon Storage. Elsevier, pp. 1–28. https://doi.org/10.1016/B978-0-12-812766-7.00001-9

Wang, J., Tu, X., Zhang, H., Cui, J., Ni, K., Chen, J., Cheng, Y., Zhang, J., Chang, S.X., 2020. Effects of ammonium-based nitrogen addition on soil nitrification and nitrogen gas emissions depend on fertilizer-induced changes in pH in a tea plantation soil. Science of The Total Environment 747, 141340. https://doi.org/10.1016/j.scitotenv.2020.141340

Wu, Yunjie, Wu, Yujie, He, P., Meng, Q., Wang, R., Zhang, M., Yuan, G., Zhao, Y., Tian, X., 2025. Spatial characteristics of soil potassium in the early stage of vegetation restoration and influencing factors in southwest China's karst region. Sci Rep 15, 2106. https://doi.org/10.1038/s41598-024-84576-w

Yang, K., Jiang, Z., Peng, H., Xin, J., Guo, B., Shen, Z., Fu, Y., Zheng, T., 2026. Elucidating soil dissolved organic nitrogen mineralization across soil depths under contrasting fertilizer-application intensities using FT-ICR MS and a two-component model. Journal of Hazardous Materials 513, 142438. https://doi.org/10.1016/j.jhazmat.2026.142438

Zhou, W., Han, G., Liu, M., Li, X., 2019. Effects of soil pH and texture on soil carbon and nitrogen in soil profiles under different land uses in Mun River Basin, Northeast Thailand. PeerJ 7, e7880. https://doi.org/10.7717/peerj.7880